Algorithm theoretical basis for Dynamic Surface Water Extent from Harmonized Landsat-8 and Sentinel-2A/B (DSWx-HLS)

John W. Jones[1], Gustavo H.X. Shiroma[2], Alexander L. Handwerger[2], Bruce C. Chapman, Charles Z. Marshak[2], David P.S. Bekaert[2], Heresh Fattahi[2], Karthik Venkateramani[2], Matthew Bonnema[2], Nicholas W. Arena[2], Renato P.M. Frasson[2], Samantha C. Neimoeller[2], Simran C. Sangha[2], Steven Chan[2]

[1]Remote Sensing Hydrology Branch, US Geological Survey
[2]Jet Propulsion Laboratory, California Institute of Technology

Corresponding Author: John W. Jones (jwjones@usgs.gov)

Key Points:

- Use of harmonized inputs affords highest temporal resolution and spatial coverage possible.
- Subpixel scale inundation is also targeted.
- Inundation dynamics in critical habitats are uncovered with precision that improves science, resource management, and hazard mitigation/response.

Abstract

Satellite-based monitoring of surface water extent provides an unequaled, comprehensive view of the global distribution of surface water. The Dynamic Surface Water Extent from Harmonized Landsat Sentinel-2 (DSWx-HLS) algorithm generates data that indicate whether surface water is present at the time of input image collection with a spatial resolution of single image pixels. The algorithm accentuates and exploits surface reflectance differences exhibited among water and other land covers across various portions of the light spectrum. The algorithm targets open surface water, pixels entirely covered by water only, as well as partial surface water, cases where water, vegetation, and soil are present at subpixel scale. DSWx-HLS tests rely on several indices calculated from the input surface reflectance bands. The algorithm uses data on land cover, fused from Copernicus Global Land Cover and WorldCover data, and a modification of the Copernicus Digital Elevation Model to reduce commission errors. Ten output layers provide transparency and flexibility in use, supporting a broad range of applications. Verification of DSWx-HLS performance given a range of cloud cover is based on comparison against data derived from nearly coincident cloud-free high resolution satellite imagery selected through global stratified random sampling. Overall accuracies of 96% and 88% were achieved for open water and partial surface water pixels, respectively. The DSWx-HLS product is generated by the Observational Products for End-Users from Remote Sensing (OPERA) Project and distributed at no cost to the user through the National Aeronautics and Space Administration (NASA) Polar Oceans Distributive Archive Center (PO.DAAC) and NASA EarthData.

Plain Language Summary

Inland surface water is a critical resource for agriculture, industry, power generation, recreation, and household use. Earth orbiting satellites systematically collect imagery that can be used to monitor variations in surface water availability and condition. To automatically analyze these images for scientific and resource management purposes, they must be processed into information computer models can easily manipulate. This document describes the theory and procedures used to automatically convert satellite images into maps of surface water extent. The procedure and the data product created are both named Dynamic Surface Water Extent from Harmonized Landsat Sentinel, or DSWx-HLS. Other procedures used for this purpose typically only target open surface water, that is, areas completely covered by nothing but water. DSWx-

HLS also targets partial surface water, that is, individual areas (pixels) measured by the satellite sensor with water and vegetation on or above the water surface. The DSWx-HLS process creates 10 output layers that provide transparency, allowing the user to understand exactly why each pixel received its label. Having multiple layers also provides flexibility, providing choices regarding which output layer is most appropriate for real-world condition and application of interest. DSWx-HLS is available at no cost to the user through the NASA Polar Oceans Distributive Archive Center (PO.DAAC) and NASA EarthData.

Keywords: Remote Sensing, Eco-Hydrology, Floodplain dynamics, Reservoirs, Wetlands, Geomorphology-fluvial

Version Description

This is Version 1.0 of the Dynamic Surface Water eXtent from Harmonized Landsat/Sentinel-2 (DSWx-HLS) Algorithm.

1 Introduction

Inland surface water is a critical resource for agriculture, industry, power generation, recreation, and potable uses. The ability to track variations in and persistence of surface water extent facilitates our understanding of human-land-climate interactions and may improve allocation and conservation of resources. Satellite-based monitoring of surface water extent provides an unequaled, comprehensive view of the global distribution of surface water. The Dynamic Surface Water Extent from Harmonized Landsat Sentinel-2 (DSWx-HLS) algorithm generates geographic data that indicate whether surface water is present at the time of input image collection with a spatial resolution of single image pixels. Analyzed in series, multiple DSWx-HLS products afford spatially distributed representation of surface water dynamics. The DSWx-HLS algorithm and its products are designed with scientific and natural resource managers in mind – emphasizing transparency, flexibility, and utility to the greatest degree possible at landscape scale given moderate resolution multispectral satellite imagery. This document describes the DSWx-HLS algorithm as implemented for near-global processing by the NASA-funded Jet Propulsion Laboratory (JPL) project named Operational Products for End-users from Remote Sensing Analysis (OPERA). Following treatments of algorithm lineage and scientific underpinning, the required processing is described in a manner that facilitates implementation.

2 Context/Background

The need to detect and track surface water occurrence at HLS pixel resolution was recognized through various research efforts aimed at producing useful parameters for hydrologic modeling and aquatic habitat resource management given systematically collected satellite data like those from Landsat. Examples include estimation of potential surface water storage at the finest resolution possible to model effects of land use and climate change on hydrology (Jones, 2011; Viger, Hay, Jones, & Buell, 2010) and the indexing of vegetation resistance to flow in wetland environments like the Florida Everglades (Jones, 2011). The requirements imposed and experience gained by these efforts highlighted the insufficiency of methods that detect water only when it is the nearly dominant, if not the sole land cover within a pixel (termed “open water”). For these and many other applications, it is important to detect inundation when pixels may also contain vegetation, bare soils, or developed land covers.

2.1 Historical Perspective

DSWx-HLS has its roots in the original U.S. Geological Survey (USGS) Dynamic Surface Water Extent (DSWE) algorithm (Jones, 2019; USGS, 2019). Designed to be globally applicable, the required inputs for DSWE were originally limited to surface reflectance data generated from Landsat satellites and a digital elevation model (DEM), given the ready availability of DEM data in some form. The utility of data generated through the DSWE algorithm has been evaluated for a variety of applications (Ahmad, Hossain, Eldardiry, & Pavelsky, 2020; Beveridge, Hossain, & Bonnema, 2020; Bjerklie et al., 2018; Chen, Huang, Chen, & Feng, 2021; Gaines, Tulbure, & Perin, 2022; Huang et al., 2017; Owusu, Snigdha, Martin, & Kalyanapu, 2022; Perin, Tulbure, Gaines, Reba, & Yaeger, 2021, 2022; Petrakis, 2022; Rowe et al., 2021; Soulard, Walker, & Petrakis, 2020; Vanderhoof et al., 2020; Walker, Soulard, & Petrakis, 2020; Yang et al., 2021). The simplicity of the DSWE algorithm is evidenced by implementations on a variety of hardware/software systems, some of which are documented in peer-reviewed scientific literature (Ahmad et al., 2020; Beveridge et al., 2020; Bjerklie et al., 2018; Owusu et al., 2022; Petrakis, 2022; Taylor, Sullivan, Teitelbaum, Reese, & Prosser, 2022; Vanderhoof et al., 2020). The USGS Earth Resources Observation and Science (EROS) Center has generated DSWE operationally since 2019. Production has been restricted to the United States and its territories because EROS only produces DSWE using Landsat Analysis Ready Data (ARD), which are only made available for the United States at this time. Given the opportunity presented by a complete reprocessing of the US Landsat ARD Archive and forward processing of ARD using Landsat Collection 2 Level 2 scene inputs, the algorithm was revised at the USGS Hydrologic Remote Sensing Branch to use US-specific ancillary inputs to reduce errors uncovered through extensive Collection 1 DSWE data evaluation and use. The HLS-based implementation through OPERA will not provide the length of historic record afforded by the use of the entire Landsat Archive as input. However, the OPERA project presents an opportunity to operationally produce DSWE-like data (i.e., DSWx-HLS) at near-global scale from both Landsat and Sentinel-2 inputs. This greatly increases both the spatial extent and temporal frequency of surface water observations. Because the land cover data used for USGS DSWE production is not available for areas beyond the United States and its territories, for DSWx-HLS production land cover is synthesized from openly available datasets with global coverage, allowing the extension of the DSWE model to global scale with highest temporal frequency.

3 Algorithm Description

3.1 Scientific Theory

Like its predecessor DSWE, the DSWx-HLS algorithm is designed to accentuate and exploit differences in surface reflectance characteristics that are exhibited among water and other land covers (Figure 1) across various portions of the light spectrum (Jones, 2015) to evaluate surface water occurrence. Five tests drawn from scientific literature are independently applied to each pixel. Three tests (Du & Zhou, 1998; Feyisa, Meilby, Fensholt, & Proud, 2014; Ji, Zhang, & Wylie, 2009) detect open water. Two more tests (Jones, 2015, 2019) are specifically designed to detect both open water and partial surface water. Laboratory-derived water, Landsat image-derived vegetation canopy, and laboratory collected soil spectral endmembers were employed in spectral mixture modeling for DSWE test development (e.g., Figure 2, Jones 2019). Use of at-surface reflectance spectra for threshold development and algorithm input provides a physical basis for threshold selection, eliminating the need to tailor thresholds to each scene or collect scene-specific training data (Jones 2019).

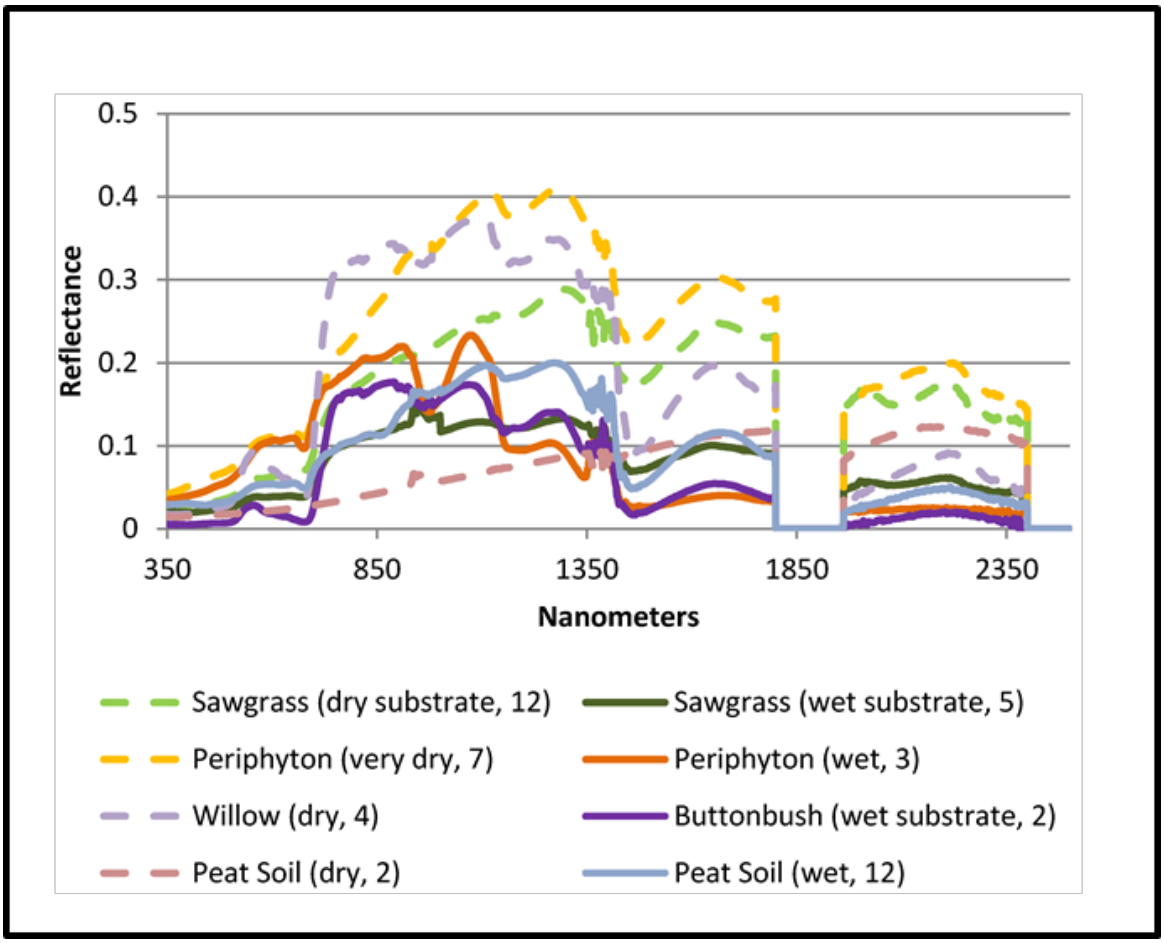

Figure 1. *Field collected, fine spectral resolution spectra of various land cover canopies and ground surfaces given both dry and inundation conditions. The influence of water substrates on reflectance across the spectrum are enhanced and exploited. The number of sampling locations per class are shown in parentheses. Spurious data around 1850 nanometers is caused by water vapor in the atmosphere, does not impact the analysis, and was removed.*

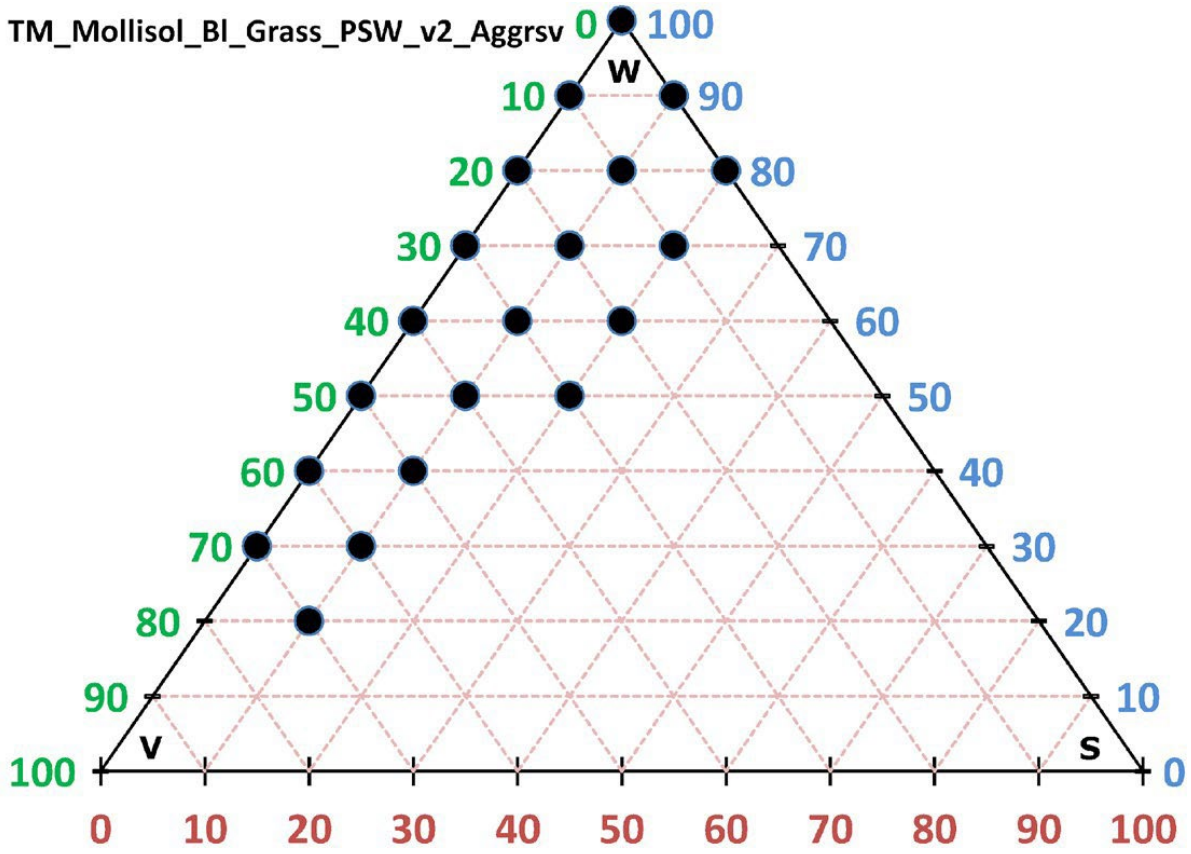

Figure 2. *Ternary diagram showing results of one partial surface water test applied against Landsat Thematic Mapper (TM) given mixtures of black soil (Mollisol_BL), herbaceous vegetation cover (Grass), and 'pure' water using the revised (v2) aggressive (Aggrsv) DSWE tests (Jones 2019). Blue axis: Water (W); Green axis: Vegetation (V); Brown axis: Soil (S). Black points represent the mixtures for which water is detected given the aggressive test. The DSWx-HLS algorithm (Figure 3) consists of a series of tests producing the intermediate (DIAG, WTR-1, WTR-2) and ancillary (CLOUD, LAND, SHAD, DEM) layers that are subsequently used to generate the final (WTR, BWTR, and CONF) product layers described and illustrated in Section 3.2.*

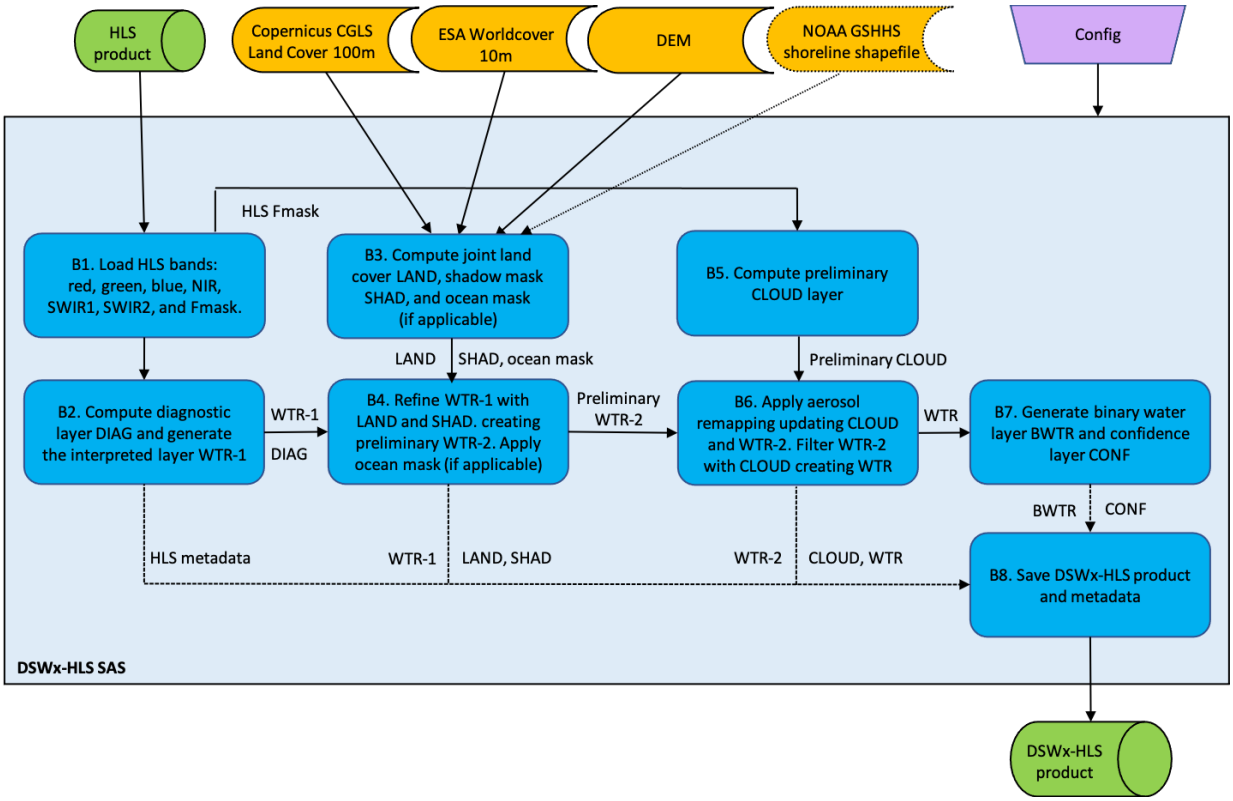

Figure 3. *At-surface Harmonized Landsat Sentinel-2 (HLS) reflectance pixels (block 1 or B1) are assigned diagnostic values (DIAG) based on detections across five tests which are then interpreted to water, partial surface water, and not water values (WTR-1) based on the combination of 'positive' detections (B2). Assembled land cover and elevation data (B3) are used in combination with HLS to conduct additional tests that reduce commission errors (B4) before HLS Fmask inputs are used to mask cloud, cloud shadow, and snow/ice covered areas (B5 and B6). A binary water layer and a layer containing confidence information related to open and partial surface water classifications are generated along with product metadata (B7 and B8).*

In combination, the layers output from DSWx-HLS allow the user to fully understand why any given pixel has been labeled to its ultimate DSWx-HLS value. Also, intermediate products can be used to improve the utility of DSWx-HLS when and where the distributed final layers (WTR, BWTR, and CONF) may be insufficient for the intended application. The five tests (Figure 3, B2) used for USGS DSWE and DSWx-HLS product generation employ at-surface reflectance or indices derived from them.

3.2 Mathematical Theory

3.2.1 Spectral Indices Calculation

The DSWx-HLS tests rely on several spectral water and vegetation indices calculated from the

input surface reflectance bands. They are calculated for each valid data pixel as indicated below using the bands described in Table 1:

Index 1: Modified Normalized Difference Wetness Index (MNDWI) (Xu, 2006):

$$(\text{Green} - \text{SWIR1}) / (\text{Green} + \text{SWIR1}) \quad (1)$$

Index 2: Multi-band Spectral Relationship Visible (MBSRV) (Du & Zhou, 1998):

$$\text{Green} + \text{Red} \quad (2)$$

Index 3: Multi-band Spectral Relationship Near-Infrared (MBSRN) (Du & Zhou, 1998):

$$\text{NIR} + \text{SWIR1} \quad (3)$$

Index 4: Automated Water Extent Shadow (AWESH) (Feyisa et al., 2014):

$$\text{blue} + (2.5 * \text{green}) - (1.5 * \text{MBSRN}) - (0.25 * \text{SWIR2}) \quad (4)$$

Index 5: Normalized Difference Vegetation Index (NDVI) (Tucker, 1979):

$$(\text{NIR} - \text{red}) / (\text{NIR} + \text{red}) \quad (5)$$

Table 1. *Harmonized Landsat Sentinel (HLS) Data are the Primary Input to DSWx-HLS.*

Band Name	OLI Band #	MSI Band #	HLS band code name L8	HLS band code name S2	Wavelength (micrometers)
Coastal Aerosol	1	1	B01	B01	0.43 – 0.45*
Blue	**2**	**2**	**B02**	**B02**	**0.45 - 0.51***
Green	**3**	**3**	**B03**	**B03**	**0.53 – 0.59***
Red	**4**	**4**	**B04**	**B04**	**0.64 – 0.67***
Red-Edge 1	-	5	-	B05	0.69 – 0.71**
Red-Edge 2	-	6	-	B06	0.73 – 0.75**
Red-Edge 3	-	7	-	B07	0.77 – 0.79**
NIR Broad	-	8	-	B08	0.78 – 0.88**
NIR Narrow	**5**	**8A**	**B05**	**B8A**	**0.85 – 0.88****
SWIR 1	**6**	**11**	**B06**	**B11**	**1.57 – 1.65***
SWIR 2	**7**	**12**	**B07**	**B12**	**2.11 – 2.29***
Water vapor	-	9	-	B09	0.93 – 0.95**
Cirrus	9	10	B09	B10	1.36 – 1.38*
Thermal Infrared 1	10	-	B10	-	10.60 – 11.19*
Thermal Infrared 2	11	-	B11	-	11.50 – 12.51*
Fmask	-	-	-	-	-

Note. Attributes of the bands provided in HLS are shown (Masek, Ju et al. 2021). Bands used in DSWx-HLS are in bold font. A single asterisk indicates values provided by Landsat Operational Land Imager (OLI) specifications and a double asterisk indicates values from Sentinel-2

Multispectral Sensing Instrument (MSI). FMASK is the HLS quality assurance layer from which snow, cloud, and cloud shadow information is drawn.

3.2.2 Diagnostic (DIAG) Layer Calculation

The following logical tests, noted by test number and an abbreviation shown in parentheses, employ the indices described above and thresholds indicated in Table 2. Negative test results in a value of 0 but the positive result of each test is assigned a unique number. Specifically, a TRUE condition resulting from tests 1, 2, 3, 4, and 5 is assigned a value of 1, 10, 100, 1,000, and 10,000, respectively. This means the combination of positive tests are efficiently noted for every pixel. The test specifics and resulting value assignments are as follows:

Test 1 (MNDWI) (Xu, 2006): Compare MNDWI to the Water Index Greater Than (WIGT) threshold: if (MNDWI > WIGT) set the ones digit (e.g., 00001)

Test 2 (MBSR) (Du & Zhou, 1998): Compare MBSRV and MBSRN values to each other: if (MBSRV > MBSRN) set the tens digit (e.g., 00010)

Test 3 (AWESH) (Feyisa et al., 2014): Compare AWESH to the Automated Water Greater Than (AWESHT) threshold: if (AWESH > AWESHT) set the hundreds digit (e.g., 00100)

Test 4 (PSW1) (Jones, 2019): Compare the calculated values of MNDWI and NDVI along with the input NIR and SWIR1 band values to their respective thresholds: if (MNDWI> PSWT_1_MNDWI & SWIR1 < PSWT1_1_swir1 & NIR < PSWT_1_nir & NDVI < PSWT_1_ndvi) set the thousands digit (e.g., 01000)

Test 5 (PSW2) (Jones, 2019): Compare the MNDWI along with the Blue, NIR, SWIR1, and SWIR2 bands to the following thresholds: if (MNDWI > PSWT_2_MNDWI & Blue < PSWT_2_blue & SWIR1 < PSWT_2_swir1 & SWIR2 < PSWT_2_swir2 & NIR < _2_nir) set the ten-thousands digit (e.g., 10000)

DSWx-HLS efficiency comes from test reliance on at-surface reflectance and index thresholds. The threshold names, brief descriptions, theoretical range, and value used for DSWx-HLS test purposes are indicated in Table 2.

Table 2. *Threshold values (Value) applied in the DSWx-HLS tests.*

Threshold Name	Description	Range	Value
WIGT	Modified Normalized Difference Wetness Index (MNDWI)	-1 to 1	0.124
AWESHT	Automated Water Extent Shadow	-2 to 2	0.0
PSWT_1_MNDWI	Partial Surface Water Test-1 MNDWI	-1 to 1	-0.44
PSWT_1_NIR	Partial Surface Water Test-1 Near Infrared	0 – 10,000	1,500
PSWT_1_SWIR1	Partial Surface Water Test-1 Shortwave Infrared 1	0 – 10,000	900
PSWT_1_NDVI	Partial Surface Water Test-1 Normalized Difference Vegetation Index	-1 to 1	0.70
PSWT_2_MNDWI	Partial Surface Water Test-2 MNDWI	-1 to 1	-0.5
PSWT_2_BLUE	Partial Surface Water Test-2 Blue	0 – 10,000	1,000
PSWT_2_NIR	Partial Surface Water Test-2 Near Infrared	0 – 10,000	2,500
PSWT_2_SWIR1	Partial Surface Water Test-2 Shortwave Infrared 1	0 – 10,000	3,000
PSWT_2_SWIR2	Partial Surface Water Test-2 Shortwave Infrared 2	0 – 10,000	1,000
LCMASK_NIR	Land Cover Mask Near Infrared	0 – 10,000	1,200

Note. Single-band threshold values are expressed in reflectance scaled similarly to the HLS inputs (scale factor is 0.0001). Where band ratios are generated, decimal threshold values are indicated.

The result of this process is the “diagnostic layer’ (DIAG), which constitutes the foundation of the DSWx-HLS algorithm. DIAG values range from 0 to 11,111, corresponding to no positive water test results, to all water tests are positive, respectively. A granule centered on Los Antiguos along the border between Chile and Argentina, South America is used here to illustrate the DSWx-HLS input surface reflectance bands and output layers. A false color composite of the focus area within the granule is provided as Figure 4. The corresponding DIAG layer output is provided as Figure 5.

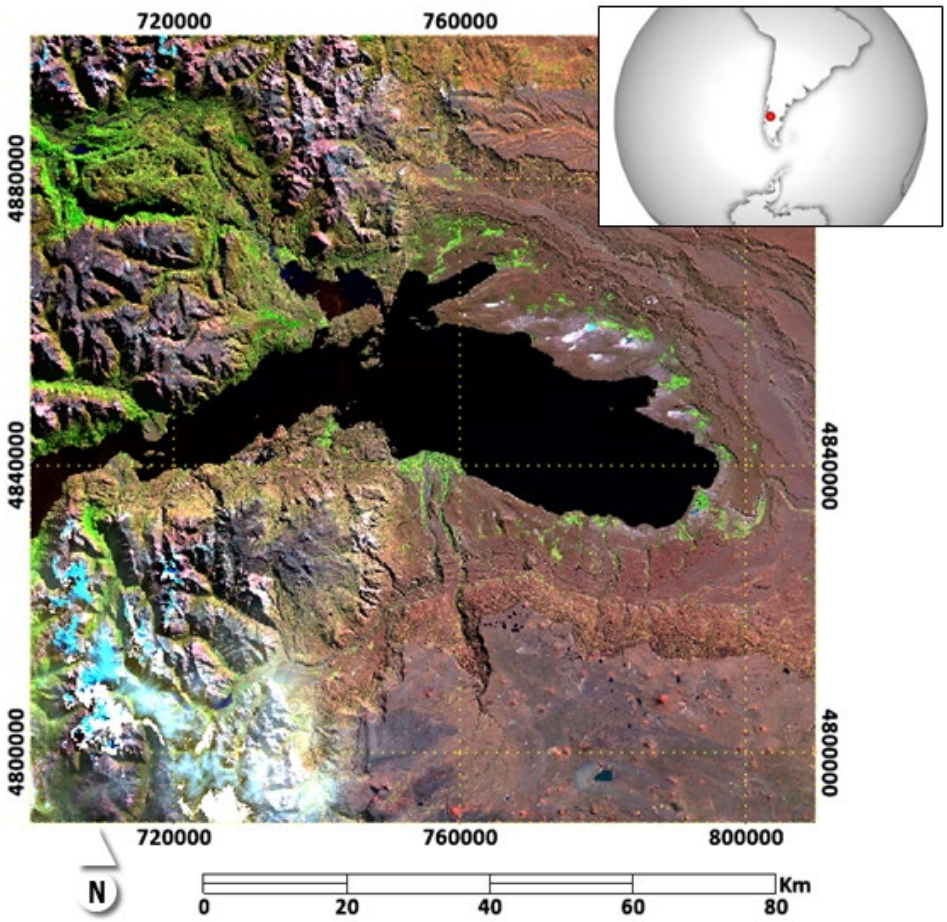

Figure 4. *False color composite (R: SWIR1: G: NIR: B: Green) for a HLS granule (OPERA_L3_DSWx-HLS_T18GYP_20230426T142425Z_20230428T080624Z_L8_30_v1.0) centered on Los Antiguos, on the border of Chile and Argentina. Coordinates shown are UTM Northings and Eastings. Subsequent figures illustrating DSWx-HLS output layers are for the same area and from this HLS input.*

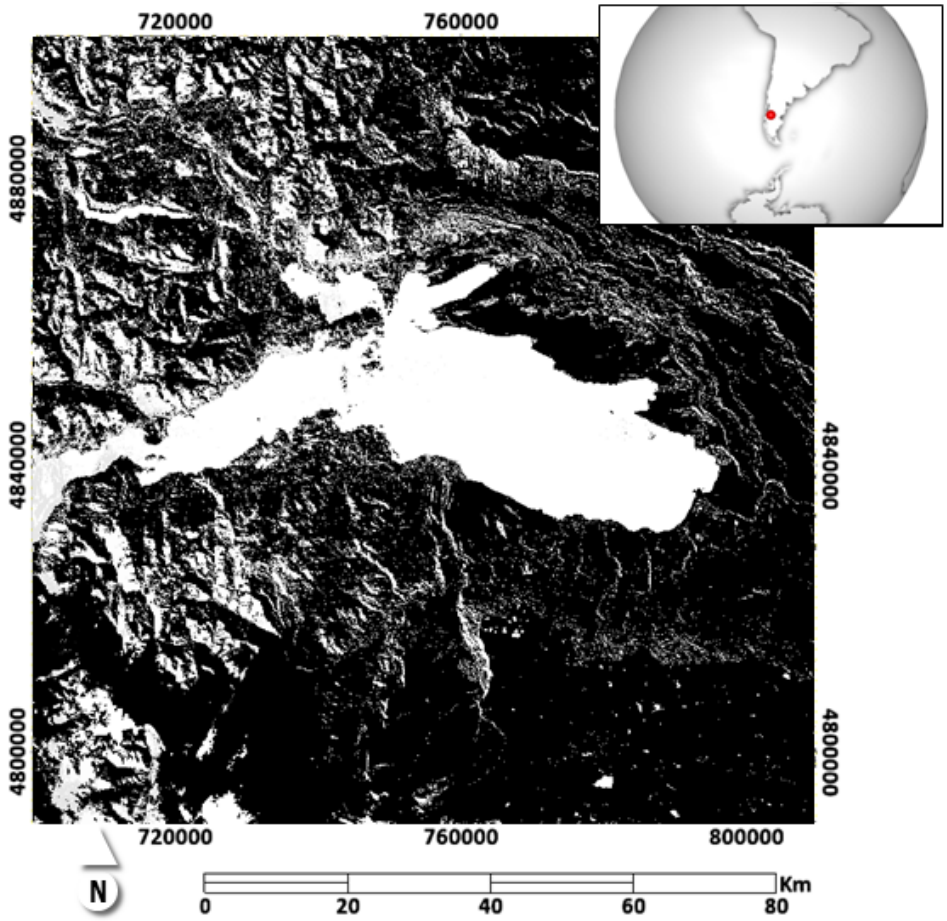

Figure 5. *Diagnostic layer (DIAG) shown in grayscale given the above HLS input. Black areas are 0 (not water), grey areas have values above 0 and below 10,000, and white areas have diagnostic values above 10,000. Coordinates shown are UTM Northings and Eastings.*

3.2.3 Interpreted Layer WTR-1 Calculation

Next, the DIAG values are interpreted to "not water", "open water", or "partial surface water" categories with initial confidence attributes (Table 3, CONF Value columns). The two tests specifically designed for partial surface water detection were originally quantitatively assessed by Jones (2019). The Partial Surface Water class nomenclature reflects the difference in the modeled minimum amount of water deemed deductible through each test (Jones 2019) as well as the acceptance of fewer positive test results in an effort to fully capture inundation. The assignment of all confidence attribute values was originally calibrated through examination of USGS DSWE times series data over 117 study areas spread throughout the US states and territories. They were further checked during DSWx-HLS calibration. The five confidence classes are: Not Water (0); Open Water High Confidence (1); Open Water Moderate Confidence

(2); Partial Surface Water Conservative (3); and Partial Surface Water Aggressive (4). To reduce complexity and facilitate concerted use of multiple DSWx products given subsequent releases of DSWx based on various synthetic aperture radar (SAR) systems, the pairs of water classes are further collapsed into a single open water and single partial surface water class (Table 3, column headings). The generated output is the interpreted layer named WTR-1. An example based on the diagnostic data shown in Figure 5 is provided as Figure 6. Note that the CONF values are incorporated in the CONF layer described in Section 3.2.8.

Table 3. *Diagnostic (DIAG) to confidence and interpreted DSWx-HLS value conversion.*

WTR WTR-1 WTR-2 Not Water value of 0	**CONF Value**	**WTR WTR-1 WTR-2 Open Water value of 1**	**CONF Value**	**WTR WTR-1 WTR-2 Partial Surface Water value of 2**	**CONF Value**
00000	0	01111	1	11000	3
00001	0	10111	1	00011	4
00010	0	11011	1	00101	4
00100	0	11101	1	00110	4
01000	0	11110	1	01001	4
		11111	1	01010	4
		00111	2	01100	4
		01011	2	10000	4
		01101	2	10001	4
		01110	2	10010	4
		10011	2	10100	4
		10101	2		
		10110	2		
		11001	2		
		11010	2		
		11100	2		

Note. Rows below the header are diagnostic values. Columns labeled CONF Value show diagnostic-confidence classes. Interpreted values shown in all column headings that include "WTR" show diagnostic - interpreted value relationships. Note that a value of 255 is inserted where the HLS input value is 'Fill'. The five confidence classes are: Not Water (0); Open Water High Confidence (1); Open Water Moderate Confidence (2); Partial Surface Water Conservative (3); and Partial Surface Water Aggressive (4).

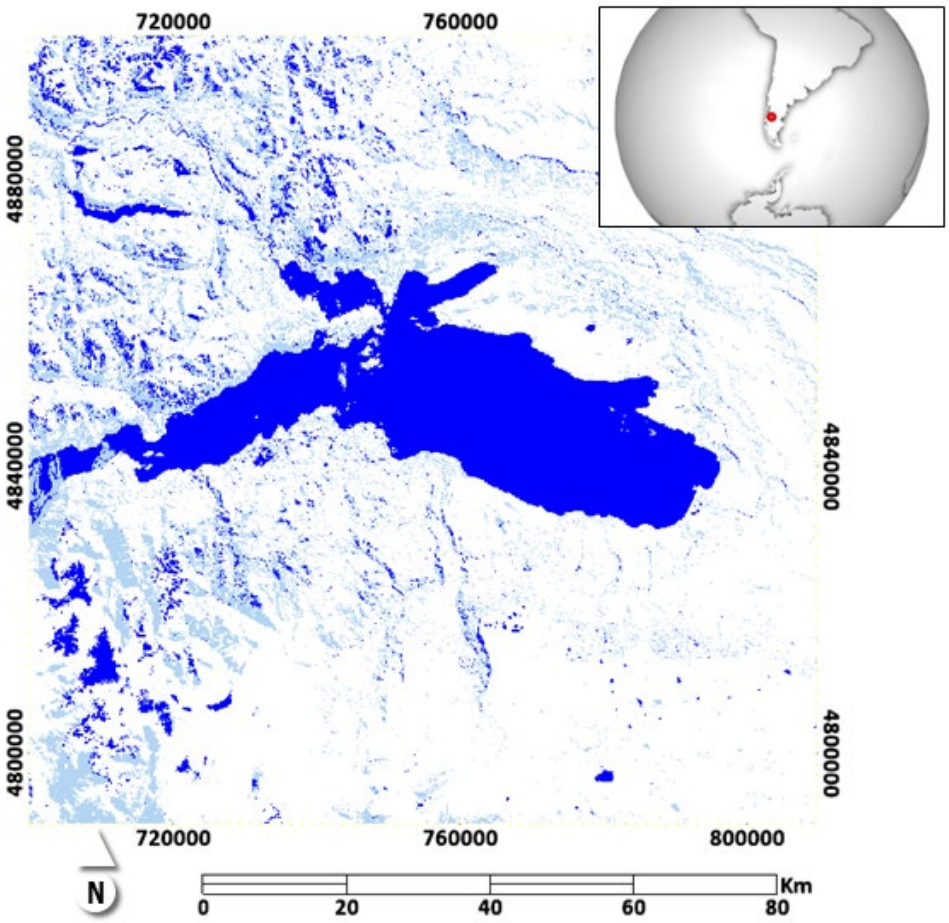

Figure 6. *The interpreted WTR-1 layer output as a result of reclassifying the diagnostic values with the scheme listed in Table 3, modified through global calibration. Open Water: dark blue. Partial Surface Water: light blue. Not water: white. Coordinates shown are UTM Northings and Eastings.*

This WTR-1 result is further processed to eliminate false positives due to terrain shading, aerosol overcorrection mitigation, certain land cover conditions, and cloud or cloud shadows.

3.2.4 WTR-2 Calculation

Particular land covers, such as large, flat, tar rooftops, or irregular evergreen forest canopies with shadows between trees, are sources of commission errors or 'false positive' detections of water. And in areas of high topographic relief, dark shadows under conditions of low sun angles are an additional source of commission errors. To reduce these errors, the algorithm generates layers for land cover (LAND) and terrain shadow (SHAD) and, based on WTR-1 values, applies additional logic. Table 4 lists the conditions considered when performing the masking of commission

errors. In the case of forest and low-to-moderate intensity development, a more conservative test of NIR surface reflectance is applied when partial surface water detections are indicated by the initial tests and diagnostic layer values. For example:

If WTR-1 = Partial Surface Water & LAND = 201 | (LAND >= 0 & LAND < 100) & NIR > 1200, set WTR-2 to "Not Water", otherwise WTR-2 = WTR-1

Where high intensity development occurs, testing has shown that shadows among tall buildings and large rooftop structures such as shopping malls and sports stadiums routinely produce false positives. For high intensity developed areas all open and partial surface water detections are masked (converted to "Not Water") before the WTR-2 layer is output. Figure 7 shows an example of the WTR-2 result when this masking is applied in the South America example area. The following subsections describe how the algorithm creates the LAND and SHAD input layers.

Table 4. Interpreted (WTR-1) Land Cover and Shadow Masking

Layer	Mask layer Class	WTR-1 Class	Other condition	WTR-2 Result
LAND	Forest	Partial Surface Water	NIR > 1200	Not Water
	Low intensity developed	Partial Surface Water	NIR > 1200	Not Water
	High intensity developed	Open Surface Water or Partial Surface Water	None	Not Water
SHAD	0 (shadow)	Open Surface Water or Partial Surface Water	LAND != water, wetland, or mangrove mask	Not Water

Note. Sequence of steps to mask the interpreted (WTR-1) layer using land cover (LAND) and shaded relief (SHAD) layers to generate the interpreted layer with some masking (WTR-2) layer. The LAND 'Forest' class is comprised of multiple Copernicus Global Land Cover forest classes. Reflectance values are shown in HLS-scaled format (e.g., 1200 = 0.12 reflectance).

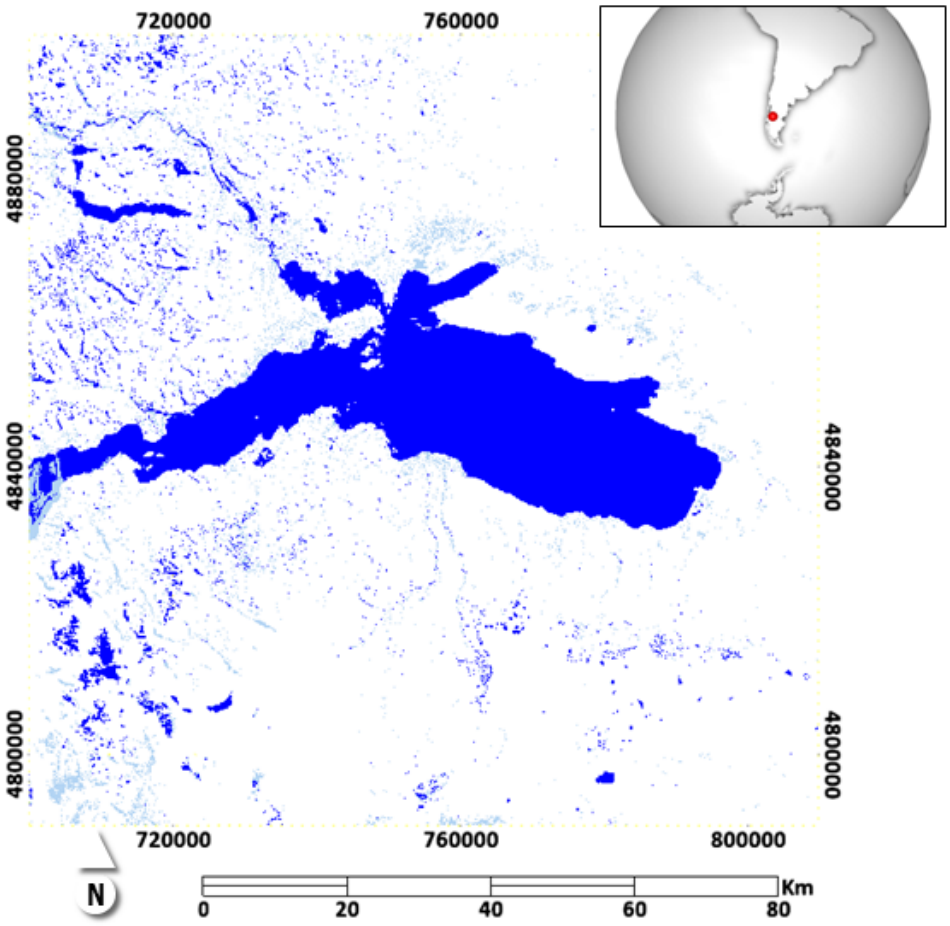

Figure 7. *The WTR-2 layer output represents a refinement, in this case very subtle, of the WTR-1 layer through masking on the terrain shadow and land cover analyses. Open Water: dark blue. Partial Surface Water: light blue. Not Water: white. The methods used to calculate the LAND and SHAD masks are detailed below and through Table 4. Coordinates shown are UTM Northings and Eastings.*

3.2.4.1 Land Cover Mask (LAND) Calculation

Land cover data are used to mitigate unwanted effects of vegetation canopies and human developed areas on water detection algorithm accuracy. The land cover mask (LAND) layer (e.g., Figure 8) is used to reduce errors through three approaches (Table 4): direct masking of

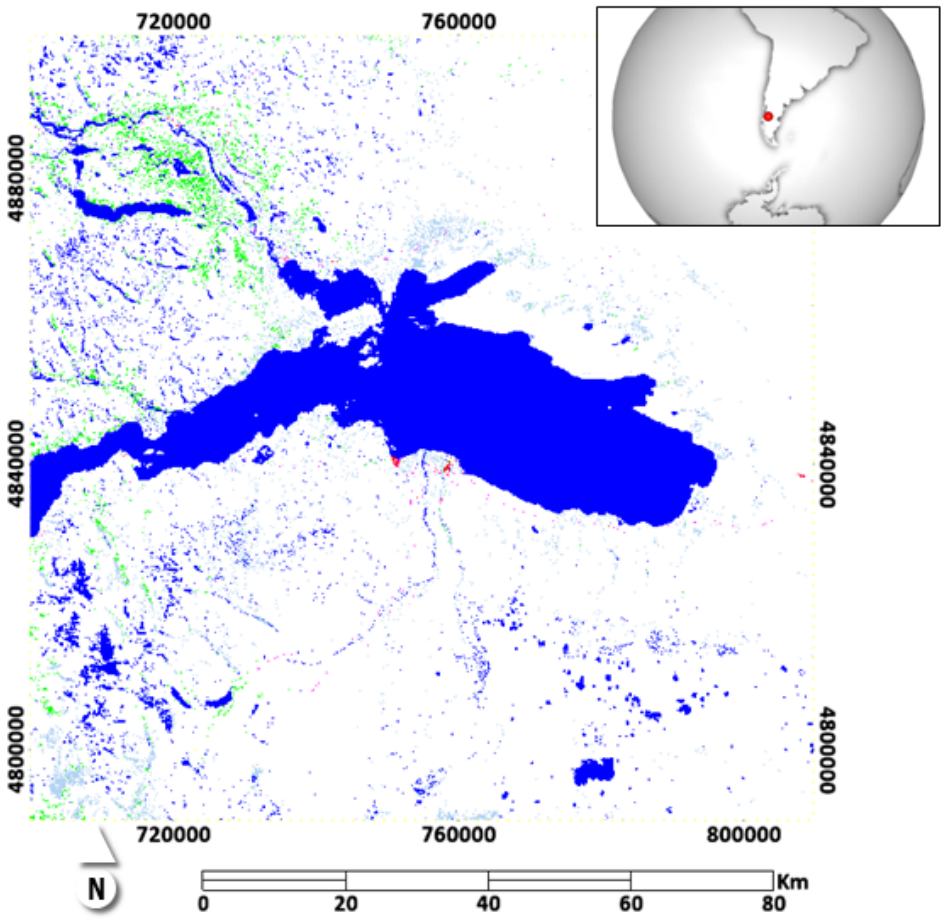

Figure 8. *The LAND layer used in the process of mitigating terrain and land cover induced false positives. Forest Cover: green; Water and Wetland: blue; High Intensity Developed: red. Coordinates shown are UTM Northings and Eastings.*

false positives; activation of additional reflectance-based testing that determines whether masking is needed to reduce false positives; and limiting the application of shadow masking (Table 4) where water or wetlands are likely to exist to reduce false negatives created by shadow masking described in Section 3.2.4.2.

National, regional, and global land cover datasets that are publicly available or available through special request were surveyed and evaluated for these purposes. Examples include: the ESA Climate Change Initiative Land Cover Maps (ESA, 2016), Moderate Resolution Imaging Spectrometer (MODIS) Land Cover Type (MCD12Q1) Version 6 (Friedl & Sulla-Menashe, 2019), Copernicus Global Land Service (Buchhorn et al., 2020), North America Environmental Atlas (CEC, 2020), various data from the Large Scale Biosphere-Atmosphere Experiment (LBA-

EDO), for example (Brown, Loveland, Ohlen, & Zhu, 2003), CORINE Land Cover (Büttner et al., 2018). No single dataset met algorithm requirements for both thematic or spatial resolution. Therefore, methods to combine several moderate and finer resolution datasets were developed and assessed through comparison with USGS National Land Cover Database (Dewitz, 2019) and USGS Land Change Monitoring and Analysis data (USGS, 2022), which are fused for USGS Collection 2 DSWE production. Ultimately, the Copernicus Global Land Service Land Cover Maps (https://land.copernicus.eu/global/index.html), which have near-global coverage with detailed thematic resolution on land cover, but coarse spatial resolution (100 m), were selected for combination with the finer 10-m spatial resolution, but lower thematic resolution of European Space Agency (ESA) WorldCover (https://esa-worldcover.org/en). This process is outlined in Figure 9 and an example from an area in the Pacific Northwest, United States, is provided (Figure 10).

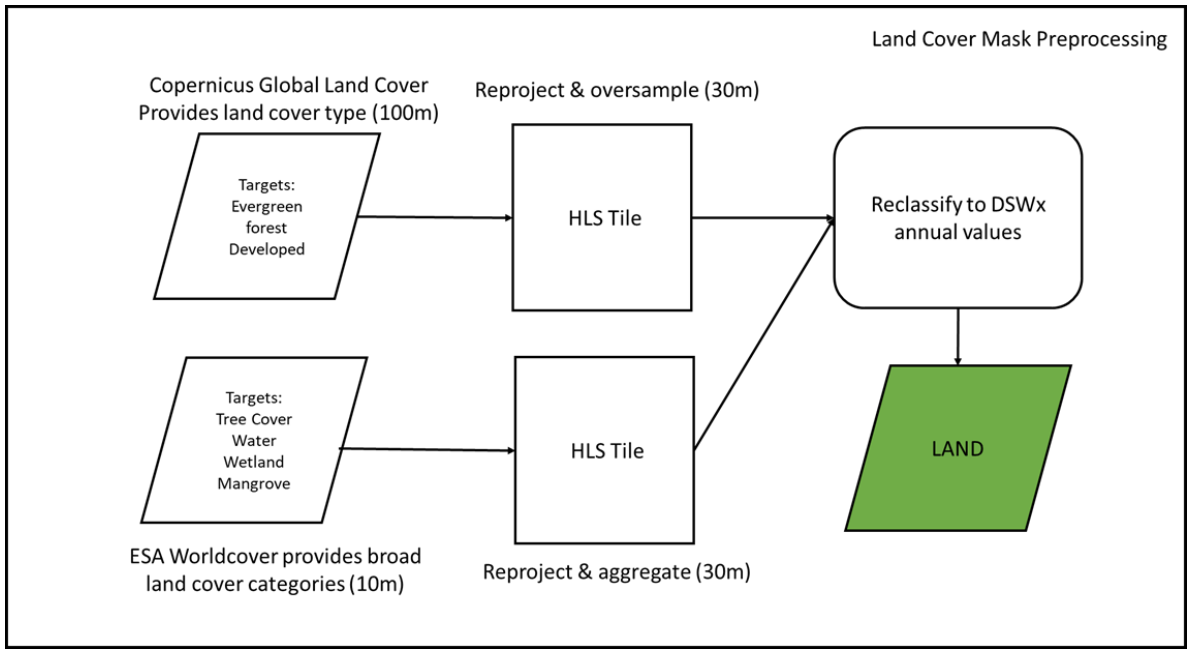

Figure 9. *Processing flow illustrating the generation of 30-m spatial resolution land cover mask data (LAND) through the combination of datasets with different thematic and spatial resolution. This layer will change as new land cover data are made available.*

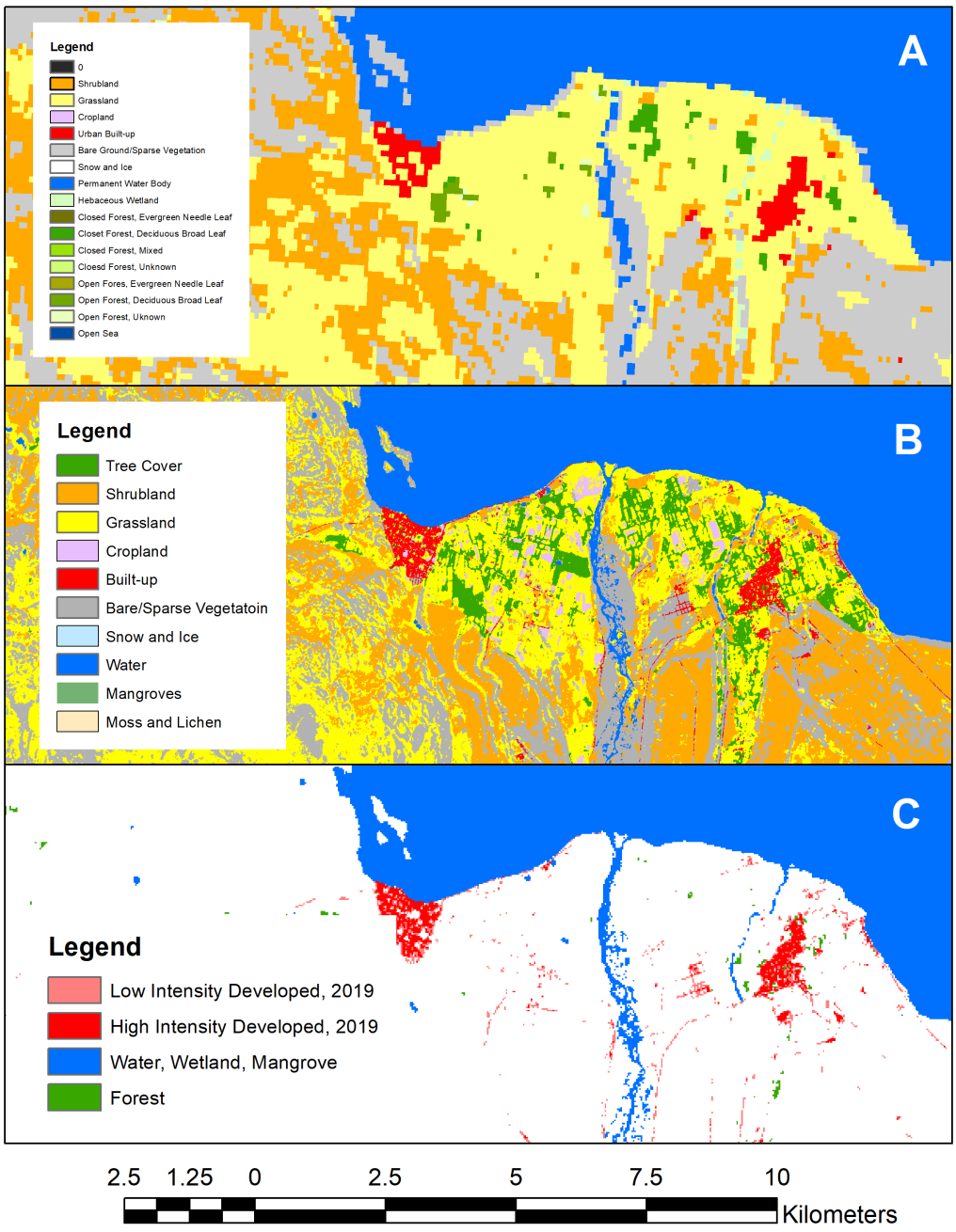

Figure 10. *A subset of the area shown in Figure 8. The legend of the Copernicus Global Service 100-m land cover (A) shows detailed thematic content that is fused with less-precise classes of ESA Worldcover 10-m data (B) using the process illustrated in Figure 9 to yield the DSWx-HLS LAND 30-m resolution land cover data (C).*

At locations that USGS DSWE calibration and application identify as challenging, iterative cross tabulations of National Land Cover Database/Land Change Monitoring, Assessment, and Projection (NLCD/LCMAP) against Copernicus/WorldCover fusions were used to establish the algorithm for aggregating WorldCover data to create forest and developed area classes based on Copernicus thematic information. This procedure was fine-tuned through the DSWx-HLS calibration process and ultimately assessed using the verification process described in Section 5. To provide for the incorporation of dynamic data on human conversion of vegetated and bare land covers to developed ones as represented in updates to the Copernicus and WorldCover datasets, developed pixels are labeled according to the last two digits of the year development appears in the data. Values 0-99 represent low intensity developed and 100-199 represent high intensity developed, potentially for the years 2000 through 2099. The land cover categories that are relevant to DSWx-HLS WTR-2 masking (forest, developed low intensity, developed high intensity, water, wetlands, and mangrove) as well as the spatial thresholds for land cover data fusion are provided in Table 5.

Table 5. LAND Layer Fusion from Various Two Inputs.

LAND Class	LAND Description	CGLC Value(s)	WorldCover Value	WorldCover threshold	Precedence
0-99	Low Intensity Developed (last two digits indicate the ESA WorldCover dataset year)	any	50	3	3
100-199	High Intensity Developed (last two digits indicate the ESA WorldCover dataset year)	any	50	7	2
200	Water, Wetland, Mangrove Forest	any	80, 90, 95	3	1
201	Non-deciduous Forest	20, 50, 111, 113, 115, 116, 121, 123, 125, 126	10	6	4
255	Fill (HLS no data)	N/A	N/A	N/A	5

Note. CGLC is Copernicus Global Land Cover. WorldCover threshold is the number of 10-m pixels in the relevant 30-m, CGLC-labeled pixel that must be present to result in the associated LAND class. N/A means 'not applicable'. The column Precedence indicates the precedence order (1 for highest) in cases where two or more conditions are met.

3.2.4.2 Terrain Shadow Mask (SHAD) Layer Calculation

Shadows produced by rugged terrain are a source of commission error for water detection algorithms. To mitigate these errors, we create a shadow (SHAD) layer to detect areas potentially affected by shadow. These areas are further evaluated along with land cover data, where areas identified as water or wetlands are removed from the masking that is applied to the WTR-1 layer (see Table 4).

We have implemented and compared two methods for detecting shadow areas. The first method is based on the solar local incidence angle and terrain slope (Shiroma, Lavalle, & Buckley, 2022). The second method is based on Otsu dynamic thresholding (Otsu, 1979). Through visual evaluation of 100 pairs of solstice and equinox examples drawn from a global, stratified random sample, the method based on the solar local incidence angle was selected as the default algorithm for creating shadow masks. In addition to having a higher accuracy with respect to the expected shadow mask, the solar local incidence angle masking thresholds need not be dynamic, which avoids the occurrence of edge artifacts between neighboring tiles that might otherwise have different shadow thresholding given the Otsu-based approach. Nonetheless, both methods are described here so that users of openly distributed DSWx-HLS code have the information needed to understand the standard (Solar Local Incidence Angle) and optional (Otsu) algorithms.

The solar geometry over the local terrain is shown in Figure 11. The solar local incidence angle θ_i is defined as the angle between the solar incidence vector $\vec{s}$ and the terrain local norm $\vec{n}$. The solar zenith θ_z is the angle between the local ellipsoid vertical $\hat{Z}$ and the solar incidence vector $\vec{s}$. The solar azimuth angle ϕ_s defines the direction of the solar incidence vector $\vec{s}$ projected over the local horizontal plane (Duffie & Beckman, 2013; Kreith & Kreider, 1978). We employ the north-clockwise convention, i.e., the angle between the North coordinate $\widehat{N}$ and the projection of the solar incidence vector $\vec{s}$ in the clockwise direction, to express ϕ_s.

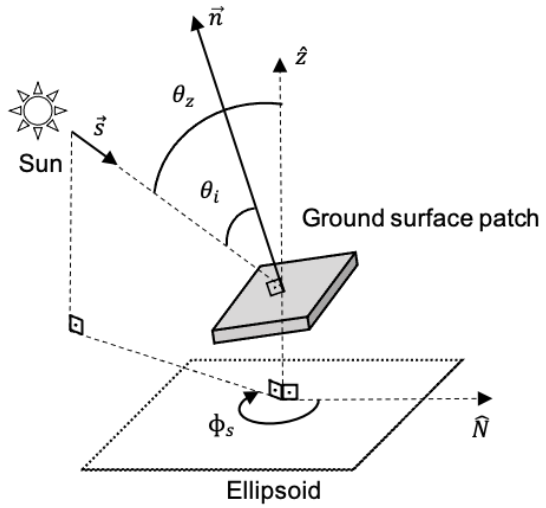

Figure 11. *Solar geometry over a ground surface patch indicating the solar angles: local incidence angle θ_i, azimuth angle ϕ_s, and zenith angle θ_z; and the vectors solar incidence vector $\vec{s}$ and the terrain local norm $\vec{n}$ referenced to the ellipsoid vertical $\hat{Z}$ and the north coordinate $\hat{N}$. (Image derived from Shiroma et al 2022).*

The input HLS product metadata provides the solar azimuth angle ϕ_s and zenith angle θ_z in local coordinates. These angles are expressed as the solar incidence vector $\vec{s}$ as:

$$\vec{s} = [sin\ \theta_z\ sin\ \phi_s,\ sin\ \theta_z\ cos\ \phi_s,\ cos\ \theta_z] \tag{6}$$

A reference digital elevation model (DEM) is resampled over the output grid using an interpolation algorithm of choice (see Figure 12 left). We suggest using a higher-order interpolation algorithm such as bicubic or biquintic to better preserve the slope information of the input elevation model. In the sequence, we compute the terrain normal vector for each position on the output grid.

$$\vec{n} = \left[-\frac{dh}{dx}, -\frac{dh}{dy}, 1\right] \tag{7}$$

where $\frac{dh}{dx}$ and $\frac{dh}{dy}$ are the elevation derivative with respect to the X- and Y- coordinates respectively, computed over the resampled DEM grid.

The solar local incidence angle θ_i is defined as the angle between the solar incidence vector $\vec{s}$ and the terrain local norm $\vec{n}$:

$$\theta_i = cos^{-1} \frac{\vec{s} \,.\, \vec{n}}{|\vec{s}| \,.\, |\vec{n}|} \tag{8}$$

In addition to θ_i, we also compute the slope angle α with respect to the Sun (directional slope):

$$\alpha = \; tan^{-1}(n_x \, sin \, \phi_s \; + \; n_y \, cos \, \phi_s \,) \tag{9}$$

where n_x and n_y are the X- and Y-components of terrain normal vector $\vec{n}$.

The detection of shadow areas based on the solar local incidence angle θ_i consists of two conditions that must evaluate to FALSE for the pixel to be considered as shadow:

1. The solar local incidence angle θ_i is less than a threshold θ_i^{max}; and
2. The slope angle α with respect to the Sun is greater than a threshold α^{min}.

If the two conditions above evaluate to FALSE, the pixel is marked as shadow (SHAD layer value “0”); Otherwise, the pixel is marked as not shadow (SHAD layer value “1”).

The first condition tests if the local terrain surface faces the Sun having the value θ_i^{max} as the maximum angle between the solar incidence vector $\vec{s}$ and the terrain local norm $\vec{n}$ for the area to be considered “not shadow”. The second test ensures that only backslope areas with respect to the Sun can be marked as shadow. This test is used to avoid cases in which flat or even foreslope areas with θ_i greater than θ_i^{max} are marked as shadow by the first test.

A sample terrain shadow layer (SHAD) along with its respective DEM are shown in Figure 12 for an area within the states of Nevada and Arizona in the southwestern United States (HLS

dataset HLS.L30.T11SQA.2019072T181446.v2.0) that has far greater topographic relief than is present in the South America focused example used to illustrate DSWx-HLS outputs.

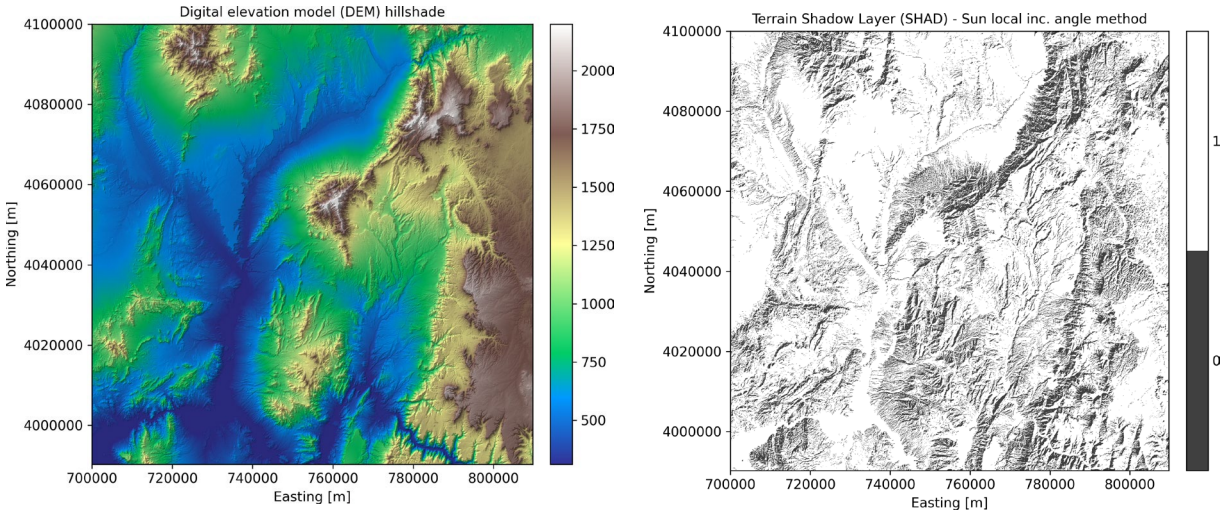

Figure 12. *(left) Hillshade of a digital elevation model (DEM) based on the Copernicus DEM 30 m, and (right) terrain shadow layer (SHAD) computed with the solar local incidence angle method for an area within the states of Nevada and Arizona, USA. In the right panel, black pixels are shadow.*

The DEM associated with the HLS image of South America that is used to illustrate all DSWx-HLS algorithm outputs is provided as Figure 13. The SHAD layer produced by the Solar Local Incidence Angle method given the solar conditions present at the time of the HLS image capture are shown in Figure 14.

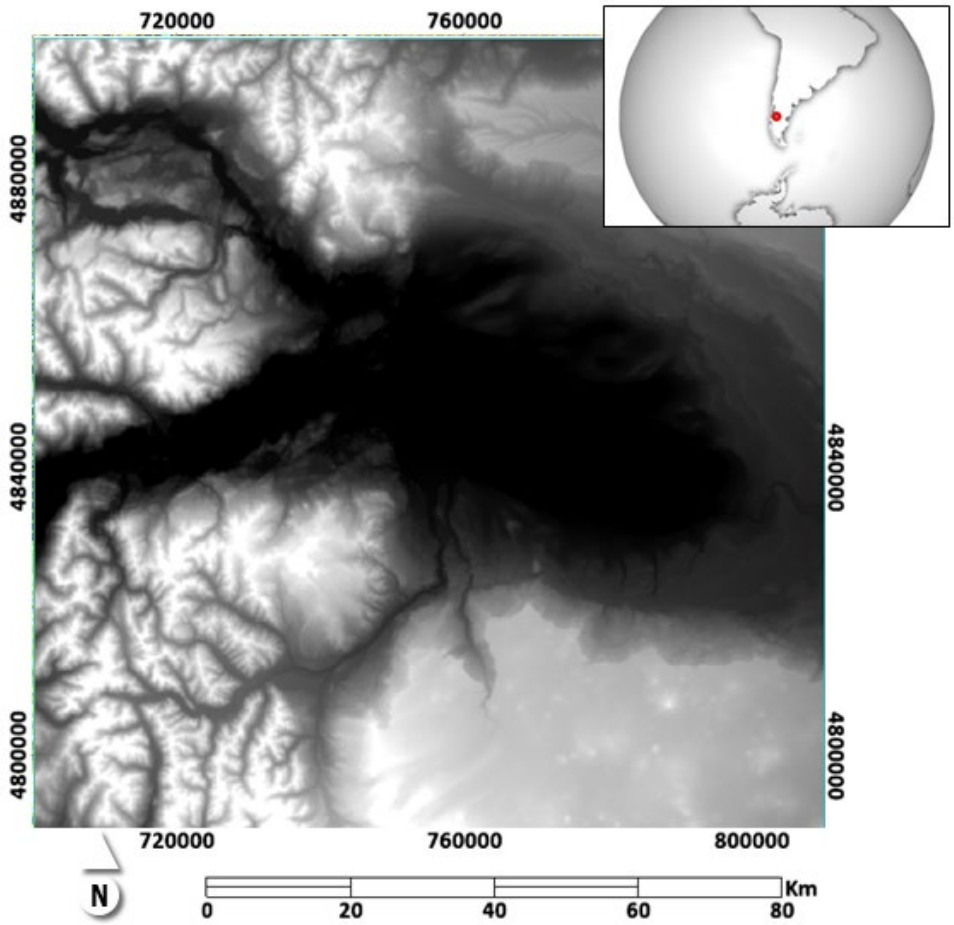

Figure 13. *The digital elevation model (DEM) for the South America sample site, used to calculate the shadow layer shown in Figure 14. Lowest elevation: black. Highest Elevation: white. Coordinates shown are UTM Northings and Eastings.*

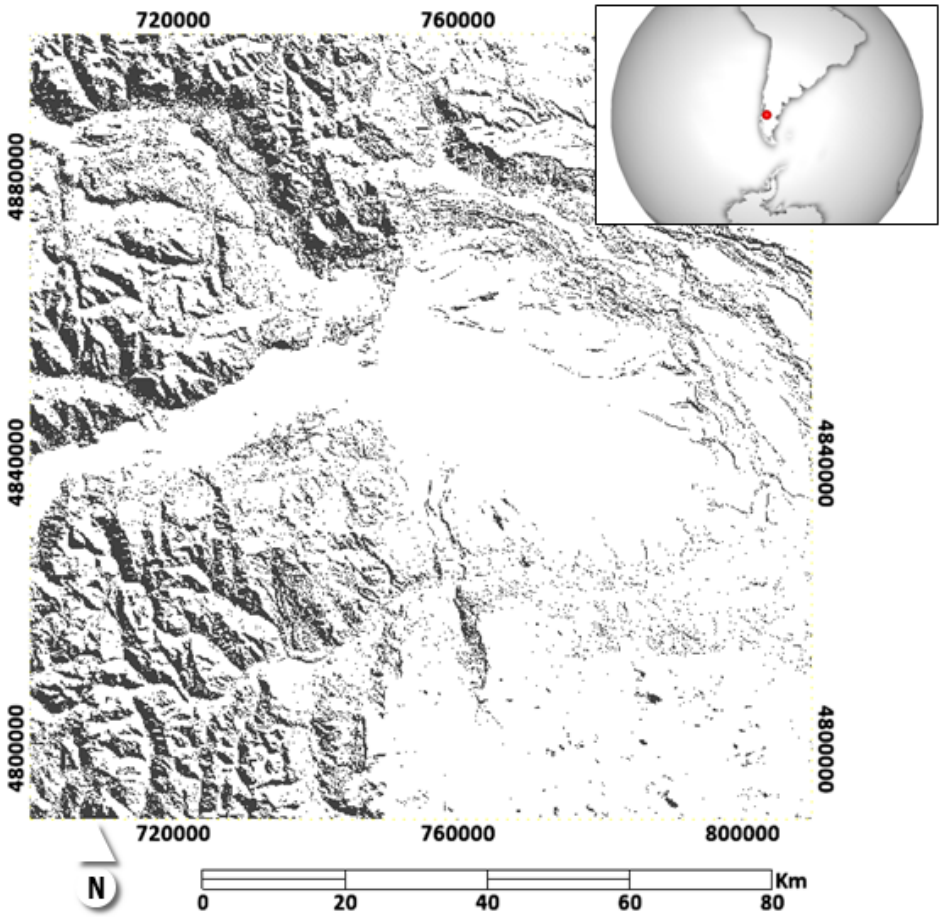

Figure 14. *The terrain shadow mask (SHAD) layer produced using the default Solar Local Incidence Angle algorithm based on the digital elevation model in Figure 13 and the solar geometry associated with the location and date/time of the example South America HLS image. Black pixels are 'shadow'.*

With the Otsu method, the location and intensity of shading can alternatively be indexed through the generation of shaded relief layers (Figure 15. left) using the scene centroid and solar angles at the time of imaging.

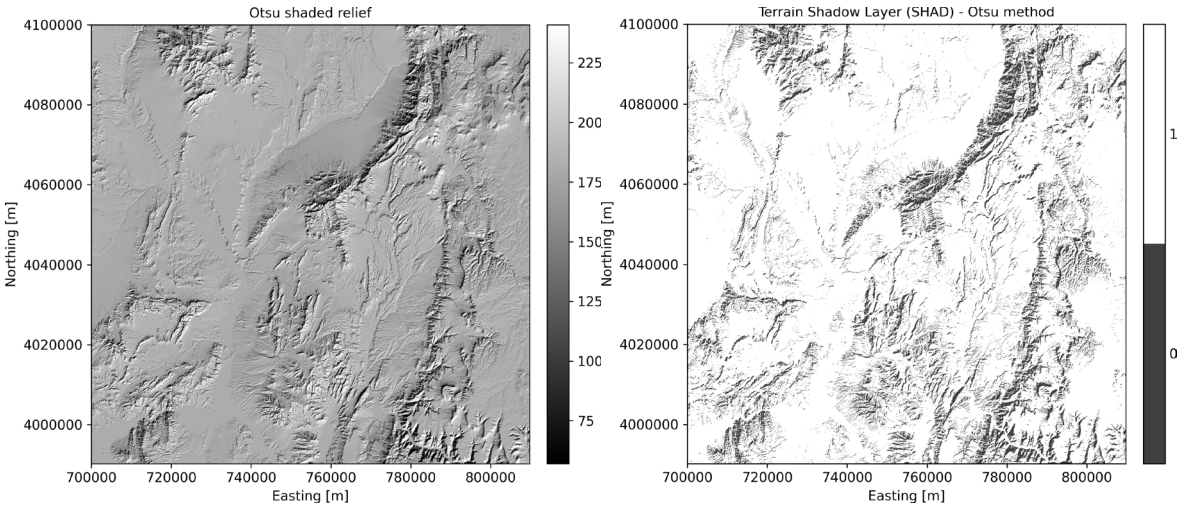

Figure 15. *Shaded relief (left) and the shadow mask (SHAD) layer (right) generated through the Otsu classification for the area within Nevada and Arizona USA that is depicted in Figure 12. In this case, the dimensionless threshold value was 146.9. In the right panel, black pixels are Shadow.*

Optional for DSWx-HLS processing, the Otsu method of automatic binary thresholding (Otsu 1979) may be used to classify the hillshade layer into two classes: shaded and not shaded (e.g., Figure 15, right). The Otsu method evaluates the histogram (frequency distribution) of grayscale images, distinguishing dark and light features in the image by determining the midpoint in the distribution among their modes. It performs best where distinct bimodal frequency distributions are present. However, this is difficult to achieve given hillshade results in areas with flat or gently undulating terrain. Prior to the calibration process, statistics on the input DEM elevations (e.g., range, standard deviation) and DEM-derived terrain characteristics (e.g., slope, aspect, and roughness) were analyzed at the tile level to distinguish which tiles should have Otsu thresholding applied.

3.2.4.2 Aerosol Overcorrection Mitigation

During global testing of the algorithm through all seasons of the year, errors were observed in DSWx pixel classifications that were error-free in USGS DSWE Collection 1. Some open water pixels were misclassified as partial surface water or not water. Further investigation identified changes to the Landsat Surface Reflectance Correction (LaSRC) processing that generates the HLS input to DSWx-HLS as the cause. Specifically, the interpolation of aerosol values over water bodies may sometimes result in pixels with unrealistically low, even negative reflectance

values in HLS. Although the partial surface water tests still frequently identify these areas as partially inundated, they are in reality open water. DSWx-HLS sample products for equinox and solstice dates for locations selected around the globe through stratified random sampling (n=98) were visually inspected for any indication of this anomaly. Some impact of the aerosol overcorrection occurred in approximately 15% of the interior (non-coastal) sites and 26% of the sites that included ocean. Therefore, an algorithm subroutine was devised to mitigate this issue until a correction to the HLS input surface reflectance can be formulated and made operational.

To avoid any need to incorporate additional ancillary data, the mitigation is based on HLS data alone. The HLS Fmask layer is consulted to determine the estimated aerosol class for each pixel and to determine which pixels are identified as 'water' by the Fmask algorithm. Testing showed that the Fmask water labeling algorithm produces commission errors along water features that are dynamic - specifically those decreasing in extent in recent times. Therefore, a DSWx-HLS decision rule that uses the HLS NIR band as an additional input was created to eliminate these commission errors. The rule applied to mitigate aerosol overcorrection impacts where WTR-1 shows 'no water' is:

> If WTR-1 is "not water" & (Fmask = 224 | Fmask = 160 | Fmask = 96) & NIR < 1000, set WTR-2 to "open water", otherwise WTR-2 = WTR-1

The rule applied to mitigate aerosol overcorrection impacts where WTR-1 shows 'partial surface water' is:

> If WTR-2 is "partial surface water" & (Fmask = 224 | Fmask = 192 | Fmask = 160 | Fmask = 128 | Fmask = 96) & NIR < 1000, set WTR-2 to "open water", otherwise WTR-2 = WTR-1

In both cases, NIR values shown are the scaled reflectance provided in the HLS product. The interpretations of the Fmask values are as follows:

> Fmask 224: Water, High Aerosol Fmask 192: High Aerosol

Fmask 160: Water, Moderate Aerosol Fmask 128: Moderate Aerosol

Fmask 96: Water, Low Aerosol

Figure 16 provides an example of DSWx-HLS WTR-2 before (left) and after the mitigation has been applied (right) for a granule centered on a lake in Ireland that exhibited the misclassification of open water due to HLS aerosol overcorrection.

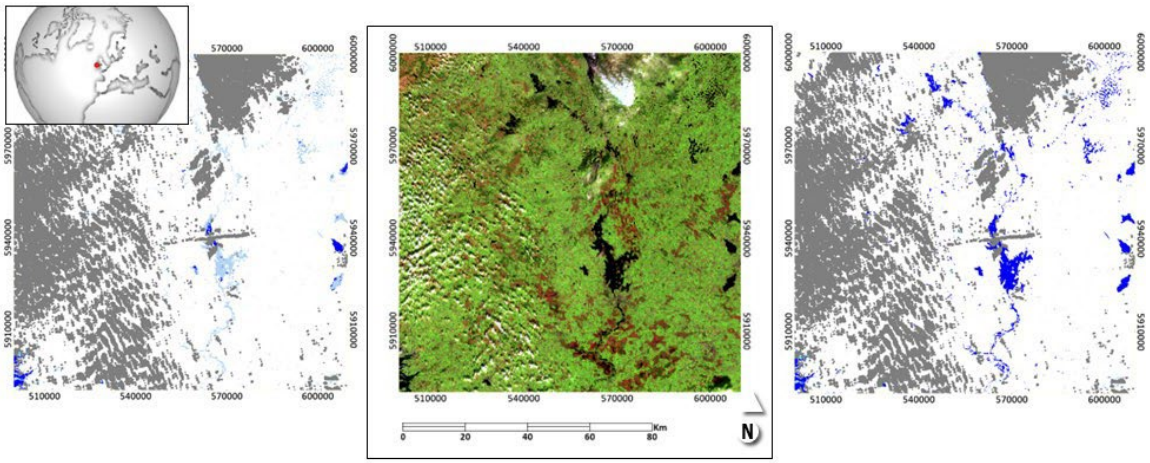

Figure 16. The WTR layer before aerosol overcorrection mitigation (left), associated HLS false color composite (R: SWIR1; G: NIR; B: Green - Middle) and mitigated/release WTR layer (right) for granule centered in Ireland. Inaccurate partial surface water (light blue in left panel) is replaced with correct open water (dark blue in right panel). White is 'not water' and gray is cloud/cloud shadow/cloud adjacent. The sample granule is the HLS scene for tile T29UNV that was collected on March 3, 2023.

3.2.5 Interpreted Layer with All Masking Applied (WTR) Calculation

Much like terrain shaded conditions, non-water covers may appear similar to water when shaded by clouds or covered by snow and/or ice. When clouds are thick enough, it is not possible to detect surface water using electro-optical satellite observations. In addition, areas around cloud/cloud shadow are often masked in surface reflectance products to further reduce the use of pixel values that may be affected by cloud cover. These are referred to as 'cloud adjacent' pixels. The bright, flat spectrum of snow is often a source of confusion for water classifiers and it is not possible to detect water under snow. To mitigate the impact of clouds, cloud shadows, cloud adjacent pixels, and snow/ice cover, the WTR-2 layer is further processed to reclassify locations identified as these features in the Fmask data provided with the input HLS surface reflectance scene. The following logical tests are applied:

If Fmask = snow/ice, set WTR = 252 otherwise WTR = WTR-2

If Fmask = cloud | Fmask = cloud shadow | Fmask = cloud adjacent, set WTR = 253 otherwise WTR = WTR-2

The output of this process is the “final water classification” (WTR) layer (Figure 17).

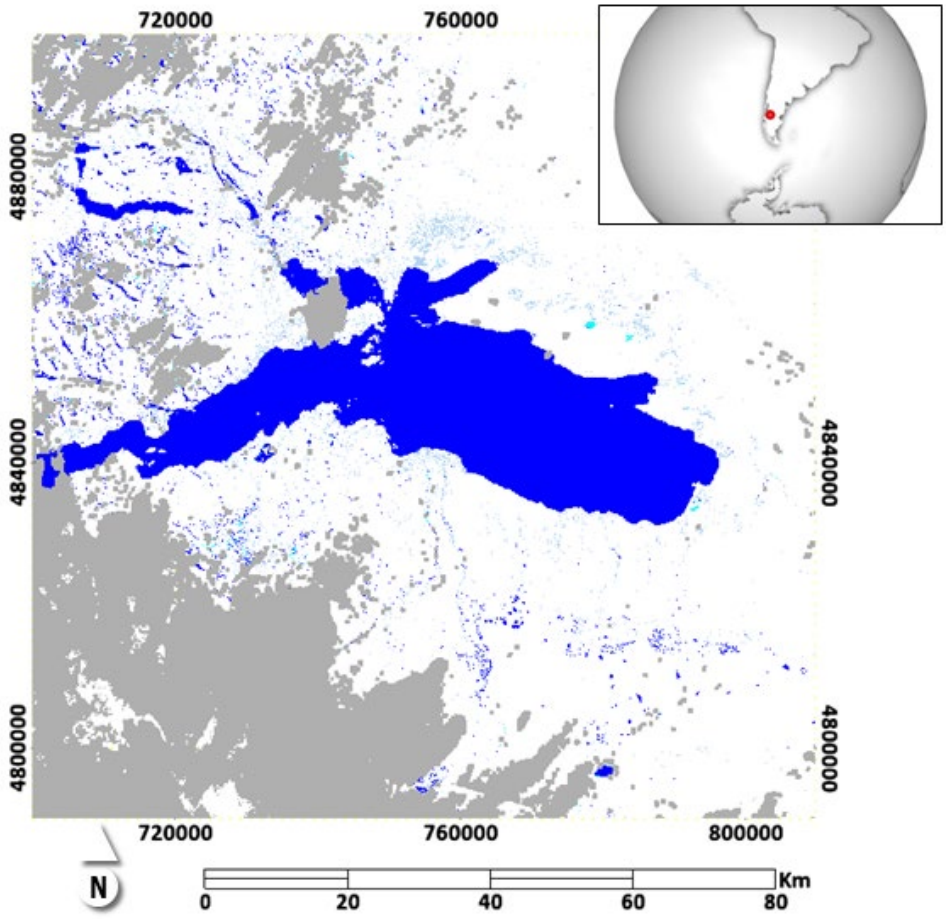

Figure 17. *The WTR layer for the South America example area. Open Water: dark blue. Partial Surface Water: light blue. Cloud, cloud shadow, adjacent to cloud: grey.*

3.2.6 Binary Layer Calculation

All water classes from the WTR layer are combined to a single water class to facilitate simplest application of the data or concerted use of future DSWx products generated from remote sensing modalities other than optical (HLS). The resulting “binary water/not water” (BTWR) Layer (Figure 18).

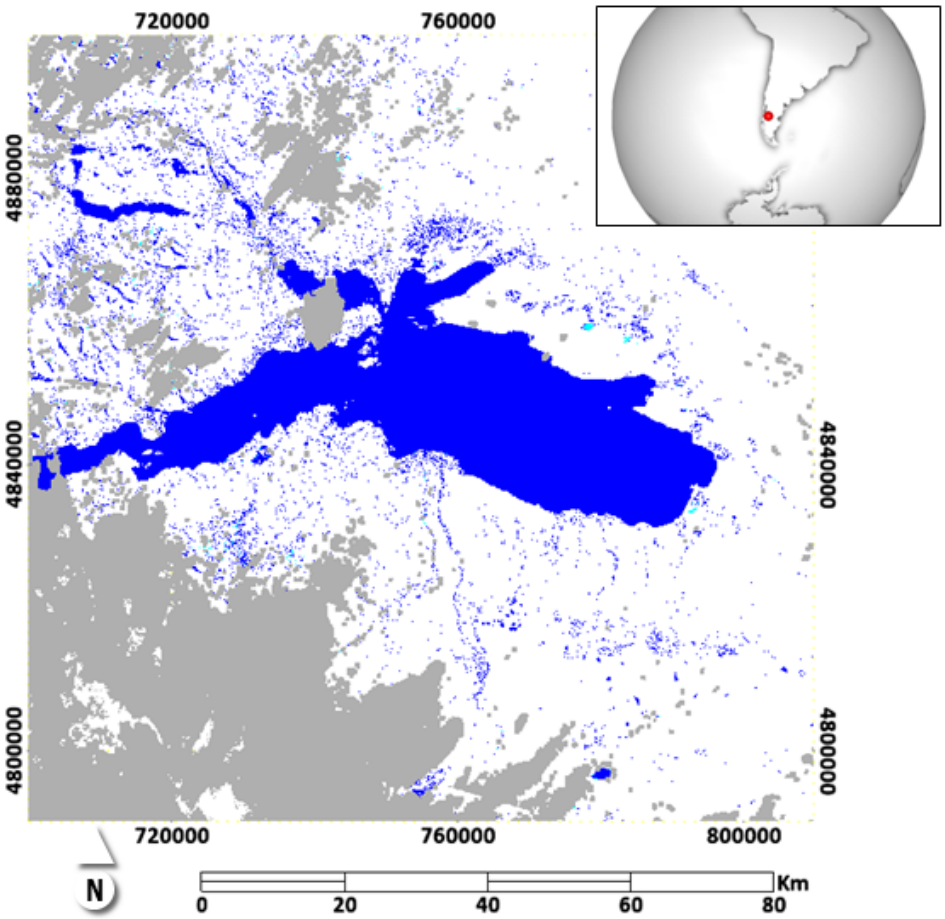

Figure 18. The binary water/not water reclassification of WTR to afford most simplistic use of DSWx- HLS output. Water: dark blue. Cloud, cloud shadow, adjacent to cloud: grey.

3.2.7 Cloud Layer Calculation

Cloud and cloud shadow masking is very difficult, particularly in the absence of thermal data, as is the case with Sentinel-2 (S30) HLS files. Snow and ice can be difficult to classify for similar reasons. The CLOUD layer indicates which pixels are snow or ice as well as which pixels are cloud, cloud shadow, and cloud adjacent to provide transparency and facilitate more sophisticated use of intermediate products. For example, in Figure 18, note that the WTR-2 layer shows valid water that was masked as cloud/cloud shadow in WTR given the input Fmask band associated with the input. For some study areas and applications, there is merit in using the WTR-2 layer in place of WTR so that less valid data are lost. Figure 19 shows the CLOUD layer for the South America example.

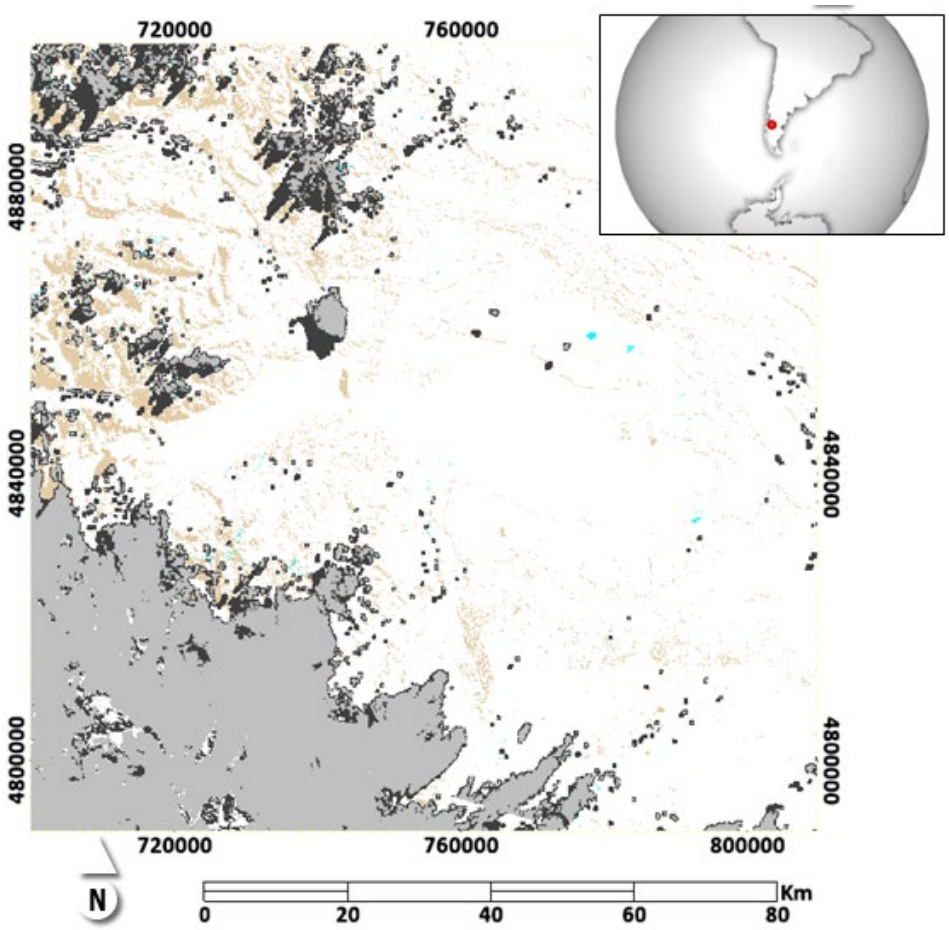

Figure 19. The CLOUD layer, which indicates cloud, snow, and water related pixel locations identified through HLS processing and provided in the HLS Fmask layer. Cloud shadow, adjacent to cloud/shadow; cloud: gray; Water: tan; and Snow/ice: cyan.

3.2.8 Confidence (CONF) Layer Calculation

The original DSWE algorithm included multiple open water and partial surface water classes differentiated on the basis of their prevalence or the aggressiveness of the water detection algorithm, respectively (Section 3.2.2). Because the OPERA DSWx product suite will eventually include data from SAR systems that may not yield multiple open and partial surface water classes, the open water high confidence and open water moderate confidence classes as well as the conservative partial surface water and aggressive partial surface water classes were collapsed into a single open water and a single partial surface water class for DSWx-HLS to facilitate harmonization across DSWx products. Although the confidence (CONF) layer lacks the simplicity of the WTR and Binary layers, it provides significant additional information for more

sophisticated and custom manipulation of the DSWx-HLS product by retaining the original water classifications. The default use of multiple hues and translucent color representation in the CONF layer further increases its utility. For example, at the inlet to the lake in the northwest corner of Figure 20, partial surface water classes, areas where water and vegetation are present within individual HLS pixels are shown in shades of green. Areas identified by the HLS Fmask algorithm as cloud/cloud shadow/adjacent to cloud along the lake in the center east section are depicted in translucent gray. DSWx-HLS often correctly identifies areas of water that were labeled as cloud during HLS Fmask processing. This symbology allows users to visualize when Fmask cloud masking is occluding valid water detections. Users have the option to use the CONF layer's calculations directly or as a guide regarding the selection of the WTR or some combination of WTR-2 and CLOUD, for example, to make best use of DSWx- HLS water detections for their study area and application. The confidence values interpreted from the diagnostic data (Section 3.2.3, Table 3) are indexed by increments of 10 to denote combinations of water, cloud/cloud shadow/cloud adjacent, and snow/ice. Table 6 illustrates the calculation of CONF layer values.

Table 6. CONF Layer Values based on DIAG, WTR-2, and CLOUD Layer Values.

Conf Class	Clear View Value	With Cloud Value (+10)	With Snow Value (+20)
Not Water	0	10	20
Open Water High Confidence	1	11	21
Open Water Moderate Confidence	2	12	22
Partial Surface Water Conservative	3	13	23
Partial Surface Water Aggressive	4	14	24

This intuitive scheme affords coding of complex combinations while minimizing the associated storage requirement.

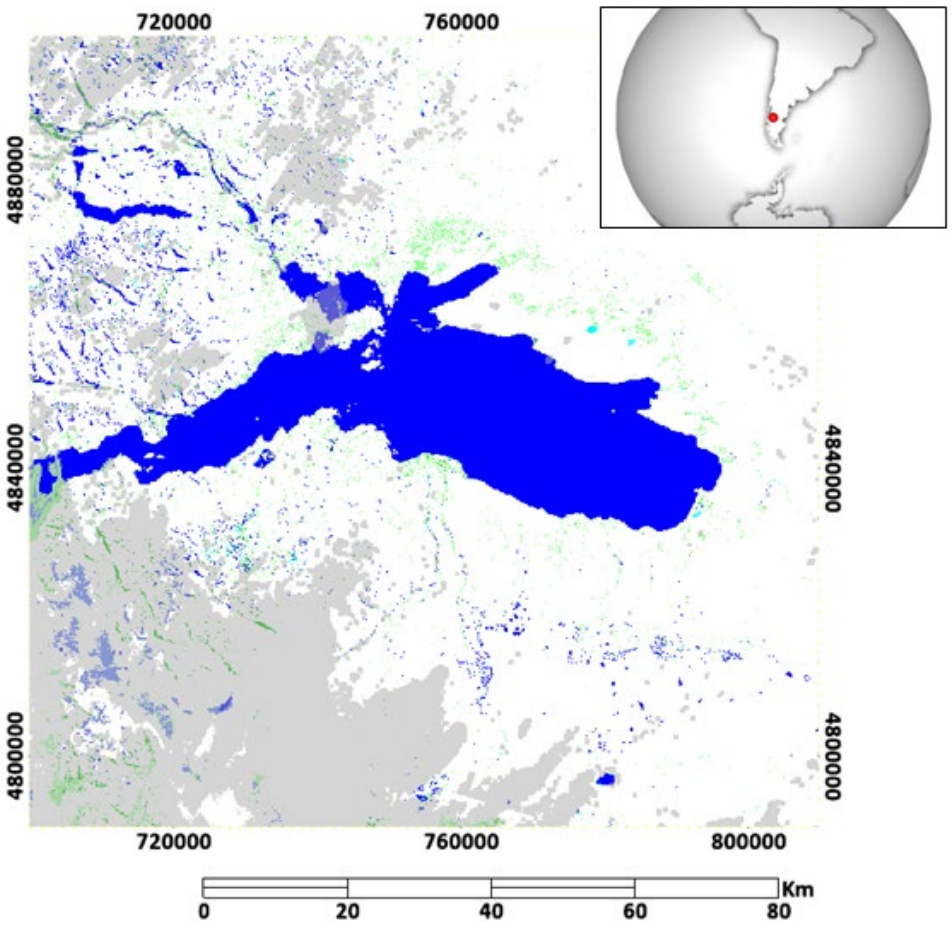

Figure 20. *The CONF layer which shows two open water classes in shades of blue and two partial surface water classes in shades of green along with translucent clouds.*

3.3 Algorithm Input Variables

The DSWx-HLS algorithm requires at-surface-reflectance data with Landsat-like bandwidths and dynamic range; a DEM, and land cover data (Table 7). The specific globally available reflectance and ancillary input files used by the DSWx-HLS algorithm are described in Table 1 (Section 3.2.1) where specifics of the input HLS band designations (Masek et al., 2021) are also provided. DSWx-HLS uses the same Sentinel-2 based military grid reference system (MGRS) projection and tiling scheme employed for HLS computation and distribution (Sentinel- 2 Level-1C product tiling grid released - Sentinel Online (esa.int)). An example of the at-surface reflectance data for a single tile is provided as Figure 4 (Section 3.2.2).

Table 7. Algorithm Input Details

Variable	Dataset	Source
Elevation	Copernicus DEM 30 m (GLO-30) and Copernicus DEM 90 m (GLO-90)	https://spacedata.copernicus.eu/collections/copernicus-digital-elevation-model
Land Cover Type	Copernicus 100-m resolution	https://lcviewer.vito.be/2015
Land Cover Intensity	ESA WorldCover 10-m resolution	https://worldcover2020.esa.int/
Surface Reflectance	Harmonized Landsat-8 Operational Land Imager (OLI) or Sentinel-2 A/B Multispectral Instrument (MSI)	https://lpdaac.usgs.gov/data/get-started-data/collection-overview/missions/harmonized-landsat-sentinel-2-hls-overview/

Analyses were conducted to select the DEM and land cover data used. Criteria for DEM selection included: open availability, timeliness, spatial resolution, geolocation accuracy, quality of elevation estimates, and performance in trial application to USGS C1 DSWE error reduction. Based upon this evaluation, the same DEM that will be used for processing of NASA-ISRO Synthetic Aperture Radar (NISAR) mission products, based on the Copernicus DEM 30 m (GLO-30-DGED) and the Copernicus DEM 90 m (GLO-90-DGED), was selected (Table 7). The DEM data are custom processed for each HLS scene to mitigate the effects of terrain shadowing as described in Section 3.2.4.2.

Land cover selection criteria included open availability, timeliness, and spatial as well as thematic resolution. No single dataset satisfactorily met both spatial and thematic resolution requirements. The process used to synthesize the DSWx-HLS LAND layer is described in Section 3.2.4.1.

3.4 Algorithm Output Variables

The algorithm results in the production of 10 separate layers in cloud optimized GeoTIFF (COG) format (Table 8). Generation of separate layers allows NASA distribution systems to provide the user with options for individual or bundled layer download. This affords significant time and storage space savings for those who choose to process DSWx-HLS outside of its ‘native’ cloud environment.

Table 8. Algorithm Output Layers.

Layer Abbreviation	Layer Long Name	Range	Data type
BWTR	Binary reclassification of WTR	0-1	Int8
CLOUD	Input HLS Fmask cloud/cloud-shadow/water classification	0-15	Int8
CONF	Confidence layer for WTR	0-24	Int8
DIAG	Diagnostic layer showing the results of each of the 5 five water tests applied to each pixel	0-11111	Int16
DEM	The digital surface model for the tile, used in the shadow mask generation (SHAD)	-	Float32
LAND	Land cover mask indicating the various land cover classes used for masking of WTR-1	0-201	Int8
SHAD	Layer showing where terrain shadow masking may be applied	0-1	Int8
WTR	Highest processed output layer (interpreted, land cover, terrain shadow, and cloud/cloud shadow masks applied)	0-253	Int8
WTR-1	Result of reclassifying 32 potential DIAG classes to three classes – termed the interpreted layer.	0-2	Int8
WTR-2	WTR-1 with terrain shadow and land cover masking applied	0-2	Int8

Note. Algorithm outputs are individual cloud optimized Geotiff (COG) files. Range does not include the default fill (no data) value possible given the HLS input, which is 255 for Int8 (8-bit integer) datasets and 65535 for Int16 (16-bit integer) datasets.

4 Algorithm Usage Constraints

The algorithm assumes the surface reflectance data generated for general land cover mapping and analysis applications are sufficiently accurate over open and partial surface water features to allow spectral mixture model-based decision rules to perform adequately. Fmask cloud, cloud shadow, adjacent to cloud/cloud shadow, and snow information is assumed accurate for purposes of final WTR classification, although the CONF and WTR-2 layers are provided to the user as alternative 'final products' when Fmask cloud/cloud shadow data hinder DSWx-HLS performance for given locations and/or applications (Section 3.2.3 and 3.2.4). The land cover mask (LAND) synthesized from two sources for masking purposes is assumed to provide adequately accurate locations of permanent water and wetlands to prevent SHAD application where surface water may be detected by the DSWx tests. LAND annual indexing of changes in

forest cover and developed area classes are assumed to have sufficient temporal resolution to capture important removal or exposure of surface water occurrences.

Algorithm performance for liquid water over non-liquid water (e.g., ice) has not been tested. Commission errors may occur on steep slopes that may not be removed through land cover masking where the Copernicus inputs to the LAND mask may suggest permanent water or wetlands exist. This has been observed in places, such as high northern or southern latitudes, and at times, such as winter, where persistent shadows exist given steep slopes and north or south-facing aspects. The algorithm cannot detect water when or where the vegetation canopy is sufficiently dense to obscure most surface water in the pixel. Cloud related and snow/ice masks inherited from Fmask may exclude areas where DSWx-HLS accurately detects water, particularly under cirrus cloud conditions or where cloud dilation to create cloud adjacent flags overestimates the impact of cloud cover.

The two algorithms for creating the terrain shadow mask presented in Section 3.2.4.2 do not include ray tracing for detecting cast shadow. Most cast shadows happen in backslope areas that are detected by the DSWx-HLS algorithm. However, some flat or fore slope areas behind steep mountains, and at high latitude during the winter season (when solar elevation is low), may be misclassified as water (commission error) due to the dark HLS reflectance.

5 Performance Assessment

Algorithm calibration and validation was baselined by the DSWx-HLS product requirements. They specify that for 80% of the validation products considered, overall accuracy must be greater than or equal to 80% for “open water” and 70% for “partial surface water” given features with a minimum area of 3 ha and minimum width of 200 m.

5.1 Validation Methods

5.1.1 Assessment Site Selection

Because inland water accounts for only 3-4% of the total inland area (Pickens et al., 2020), assessment site selection through global stratified random sampling improves efficiency and accuracy of DSWx evaluation over techniques based on random or systematic sampling alone.

The performance verification sites used for algorithm evaluation were drawn from the Pickens et. al. (2020) global stratified sample framework depicted in Figure 21. Each point was attributed with a percent water as calculated over a 240 km^2 surrounding area.

Figure 21. *Validation chip locations as selected randomly from the global sample framework of Pickens et. al. (2020). The site highlighted by green triangle along the border between Russia and Kazakhstan is the chip example shown in Figure 22. (base map data are openly available from ©OpenStreetMap and contributors).*

For DSWx-HLS performance verification, a 121 km^2 area, termed a 'chip', was delineated within each 240 km^2 area identified by Pickens et al. (2020). Next, image 'pairs' were extracted from the HLS and PlanetScope archives (https://www.planet.com/science/) for the year 2019 using several criteria. Each chip had to be covered by HLS and PlanetScope data. To provide a good indication of product performance across a broad range of applications, HLS cloud cover was allowed to vary between 0 and 60% according to HLS metadata. In contrast, to yield the highest quality verification data possible, PlanetScope image selections were limited to 'cloud free' conditions according to its metadata. Next, only PlanetScope data collected within 24-hours of acceptable HLS scenes were identified. The resulting metadatabase contains pairs of near-coincident 2019 HLS/PlanetScope images that adhere to these criteria. Chips were then randomly drawn from the database with the goal of obtaining a minimum of 10 sites in each of four strata of surface water coverage: Strata 0 (dry - 0% water, n = 10); Strata 1 (sparse > 0 and

<= 0.08% water, n = 10); Strata 2 (moderate > 0.08 and <= 2% water, n = 13), and Strata 3 (great water > 2%, n = 19). That is, each framework was repeatedly, randomly sampled without replacement until the performance verification chip database provided the desired minimum distributions of percent inundation across the four strata.

5.1.2 Evaluation Data Generation

For DSWx-HLS performance verification PlanetScope data were processed using combined automated classification, visual inspection, hand editing, independent evaluation, and subsequent revision to generate high-resolution open water masks for each chip. In practice, examination of low agreement for some DSWx/verification chip pairs sometimes led to reexamination and correction of the verification chip, as additional water was identified. Figure 22 shows an example of one PlanetScope input and the corresponding verification chip.

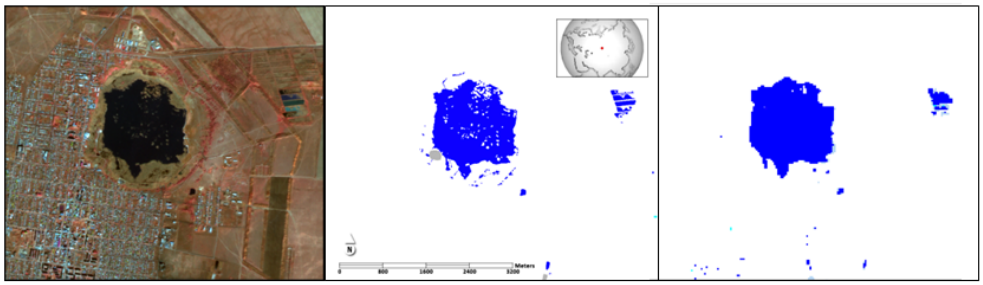

Figure 22. *A verification chip example: PlanetScope image (left); evaluation dataset derived from the PlanetScope image (center) and corresponding DSWx-HLS WTR layer (right). The PlanetScope image was collected one day after the HLS scene used for DSWx input. The location of this "truth chip" is shown as a large green dot in Figure 21.*

For the image-based comparisons, the coincident high-resolution water maps were aggregated into the projection and resolution framework of the DSWx product being evaluated. Percentages of water within each HLS pixel, based on the higher-resolution data, were estimated and pixels with greater than 50% but less than 100% open water were labeled as partial surface water pixels. Areas of cloud, cloud shadow, adjacent to cloud, or snow identified in either the DSWx-HLS or the PlanetScope evaluation data were relabeled 'no data' in both datasets. Clusters of open and partial surface water pixels in the evaluation data that were smaller in area than the 3-ha minimum mapping unit of the OPERA Project requirement were removed and any

overlapping DSWx-HLS water pixels were also eliminated. However, the 200-m minimum width requirement was not included as a filter due to the complexity and computational resources it would necessitate. The impacts of this decision are discussed in the following sections.

5.1.3 DSWx-HLS and Evaluation Product Comparisons

OPERA Project requirements reference only 'accuracy', that is the number of correct classification predictions divided by the total number of classification attempts (expressed as a percent):

$$\text{Accuracy} = (TP + TN) / (TP + FN + FP + TN) \quad (10)$$

where

TP = True Positives (class in question is shown where present)

TN = True Negatives (absence of class in question is shown where absent)

FP = False Positives (class in question is incorrectly shown as present)

FN = False Negatives (absence of class is shown where it is actually present)

To avoid extremely high, less informative accuracy values that can result from an imbalance in mapped classes, the DSWx-HLS and evaluation product values were sampled at an equal number of randomly cast points within each of the open water, partial surface water, and not water classes. This resulted in a total of approximately 1,000 samples equally divided among classes for each chip. Further, this process was repeated 100 times for each chip.

To provide additional insights, all the metrics shown in Table 9 were calculated for every execution on each chip and summarized within and across all chips.

Table 9. Performance Assessment Metrics

Metric	Definition	Formula	Notes
Accuracy	Of the total number of evaluation points, how many were correctly classified?	(TP + TN) / (TP + FN + FP + TN)	OPERA requirement. Equal sampling provides conservative accuracy estimate

Precision (P)	Of the total positive predictions, what number were correct?	TP / (TP + FP)	Not a requirement. Excludes correct 'not water' predictions that boost overall accuracy
Recall (R)	Of the total number of evaluation points, how many positive predictions were correct?	TP / (TP + FN)	Not a requirement
F1 Score	Harmonic mean of Precision and Recall	2 * P *R / (P + R)	Provides a conservative accuracy estimate

Note: These performance assessment metrics were calculated to confirm whether DSWx-HLS output meets project requirements (row 1) and to provide additional insights regarding algorithm performance (rows 2 – 4).

To verify that the algorithm met project performance requirements, accuracy was calculated separately for open surface water (OSW) and partial surface water (PSW). The additional metrics described in table 9, which provide greater insight regarding DSWx-HLS performance, were augmented with the calculation of all water classes combined, regardless of open or partial surface water designation. This provides an estimate of DSWx-HLS binary layer performance, which is provided in the standard product to facilitate harmonization across the optical (HLS) and planned SAR DSWx products. Describe the details of the scientific methods utilized for algorithm performance assessment validation. Details provided should match the current algorithm maturity.

5.2 Uncertainties

The stratified selection of sample chips provides a good range on inundation conditions and environments at near-global scale. At the individual chip scale, repeat stratified random sampling to produce mean accuracy, precision, and recall results in low uncertainty. However, where vegetation cover is particularly prevalent, for example in marsh, wet prairie, and swamp environments, it is difficult to rely on classification maps generated from high-resolution optical data alone for validation purposes. For this reason, in situ data like those from the Everglades Depth Estimation Network (Jones 2015, Jones 2019) and other field data such as wetted perimeters collected in the field (Rowe et al., 2021), will be used in direct comparisons with DSWx and to train classifications of high-resolution imagery for further evaluation of DSWx

partial surface water and water under vegetation classes. Because these types of data are difficult to compile at global scale, they will serve as evaluation rather than validation efforts.

The strength of PlanetScope as an evaluation data source is its systematic global coverage with high temporal frequency. However, there are conditions for which limited spectral range and high signal-to-noise characteristics result in errors in the 'truth data' used for performance assessment. Although each evaluation chip was independently reviewed through visual inspection and when necessary, improved through hand editing, the automated performance assessment process still identified errors in the evaluation data. Chips that 'performed poorly' were investigated in detail, through comparison with even higher spatial resolution and more spectrally robust, near coincident and/or time series data. Examples include submeter resolution MAXAR satellite or National Aerial Imaging Program (NAIP) airborne data. In several cases, the DSWx-HLS algorithm correctly detected partial surface water inundation that was misclassified as open water or not water areas using the PlanetScope data. Conversely, 'wetland' and water bodies identified in the PlanetScope data were in some cases bare ground or vegetated areas without inundation. It is possible that additional errors have yet to be uncovered, increasing the uncertainty of the performance assessment. However, these types of errors result in lower performance metric values, not higher ones. The accuracy estimates are conservative rather than optimistic.

5.3 Validation Errors

The accumulated results, shown in Table 10, demonstrate that DSWx-HLS surpassed OPERA Project requirements, even with the use of the strict, more conservative sampling approach. For open surface water, 83% of evaluation products examined passed the 80% accuracy requirement. For partial surface water, 85% met the 70% accuracy requirement. And 81% of chips evaluated had both OSW and PSW accuracies above the Project requirement threshold.

Table 10. Percentages of evaluation products for which performance requirements were met.

Class	Pass	Fail	Percent
Open Surface Water (OSW)	43	9	83%
Partial Surface Water (PSW)	44	8	85%
Both (OSW + PSW)	42	10	81%

Table 11 shows the statistics regarding all metrics calculated across several treatments. The top

section of the table includes all chips in the calculation of the metrics. The second section includes only those chips that individually passed the performance metrics.

Table 11. Performance metrics statistics by treatment, that is, the DSWx-HLS class(es) being evaluated.

Treatment	Metric	Mean	Median	St. Dev.
All chips (n=52)				
OSW, PSW, and NW	Accuracy (%)	88.03	90.85	12.93
OSW	Accuracy (%)	96.13	98.90	5.97
	Precision (%)	84.23	92.55	17.95
	Recall (%)	95.54	100.0	13.65
	F1 (%)	97.96	93.41	14.08
PSW	Accuracy (%)	88.35	90.88	12.42
	Precision (%)	70.64	82.06	34.01
	Recall (%)	60.09	91.31	42.97
	F1 (%)	50.56	43.54	40.7
Passing chips (n=42)				
OSW	Accuracy (%)	97.02	99.38	0.05
	Precision (%)	90.00	100	0.06
	Recall (%)	95.60	100	0.00
	F1 (%)	92.00	1	0.06
PSW	Accuracy (%)	93.05	97.67	0.08
	Precision (%)	90.45	100	0.06
	Recall (%)	71.81	100	0.00
	F1 (%)	58.45	74.5	0.12

When only sites that pass the requirement threshold are considered (42/52 or 81%), OSW mean accuracy is 95%, and PSW mean accuracy is 92%, indicating that under the majority of circumstances, accuracy is substantially higher than the averages would indicate. The minimum width requirement for features (i.e., 200 m) was not imposed in this analysis, which reduces DSWx-HLS performance metric values.

6 Algorithm Implementation

6.1 Algorithm Availability

The DSWx-HLS algorithm is currently implemented in the PROTEUS toolbox, which is open, and can be accessed through the following GitHub repository: https://github.com/opera-adt/PROTEUS

6.2 Input Data Access

Input data sources are described and provided in Section 3.3 and Table 7.

6.3 Output Data Access

DSWx-HLS output is openly available at no cost to the user through NASA EarthData and the NASA PO.DAAC.

6.4 Important Related URLs

The OPERA DSWx Product Suite (DSWx Product Suite (nasa.gov)) provides links to all DSWx-HLS documentation and data access.

7 Significance Discussion

DSWx-HLS targets subpixel inundation at Landsat resolution, uncovering significantly more water than is detected than through open water algorithms alone. DSWx-HLS efficiently and systematically generates near-global coverage of the highest temporal resolution, finest spatial resolution data available on open and partial surface water dynamics.

8 Open Research

The DSWx-HLS algorithm is currently implemented in Python in the PROTEUS toolbox. The source code of the PROTEUS toolbox is open and it can be accessed through this GitHub repository: https://github.com/opera-adt/PROTEUS. All evaluation data and python code related to their analyses are openly available through this GitHub repository:

.

9 Acknowledgements

Batuhan Osmanoglu and Grace Bato's efforts to engage DSWx-HLS stakeholders and potential users are gratefully acknowledged. Funding support for this work was provided by the NASA IMPACT and USGS National Land Imaging Programs.

Contact Details

John W. Jones

John Jones (0000-0001-6117-3691) - ORCID

jwjones@usgs.gov

Roles: conceptualization; methodology, validation, formal analysis; investigation; writing - original draft; writing -review and editing; visualization, supervision, funding acquisition

Affiliation: U.S. Geological Survey, Kearneysville, WV, USA

Gustavo H.X. Shiroma

Gustavo Hiroshi Xavier Shiroma (0000-0002-7753-1876) - ORCID

gustavo.h.shiroma@jpl.nasa.gov

Roles: formal analysis; investigation; software; writing – original draft; writing -review and editing;

Affiliation: Jet Propulsion Laboratory, California Institute of Technology, Pasadena, CA, USA

Alexander L. Handwerger

https://orcid.org/0000-0001-9235-3871

alexander.handwerger@jpl.nasa.gov

Roles: validation, investigation, software

Affiliation: Jet Propulsion Laboratory, California Institute of Technology, Pasadena, CA, USA

Bruce C. Chapman

https://orcid.org/0000-0002-6054-7695

bruce.d.chapman@jpl.nasa.gov

Role: supervision

Affiliation: Jet Propulsion Laboratory, California Institute of Technology, Pasadena, CA, USA

Charles Z. Marshak

Charlie Marshak (0000-0001-5633-7153) - ORCID

Charlie.z.marshak@jpl.nasa.gov

Roles: validation, investigation, software

Affiliation: Jet Propulsion Laboratory, California Institute of Technology, Pasadena, CA, USA

David P.S. Bekaert

david.bekaert@jpl.nasa.gov

Roles: supervision, project administration, funding acquisition

Affiliation: Jet Propulsion Laboratory, California Institute of Technology, Pasadena, CA, USA

Heresh Fattahi

heresh.fattahi@jpl.nasa.gov

Roles: supervision, funding acquisition

Affiliation: Jet Propulsion Laboratory, California Institute of Technology, Pasadena, CA, USA

Karthik Venkataramani

https://orcid.org/0000-0003-2712-9210

karthik.venkataramani@jpl.nasa.gov

Roles: validation, investigation

Affiliation: Jet Propulsion Laboratory, California Institute of Technology, Pasadena, CA, USA

Matthew Bonnema

matthew.g.bonnema@jpl.nasa.gov

Roles: validation, investigation, software, data curation, visualization

Affiliation: Jet Propulsion Laboratory, California Institute of Technology, Pasadena, CA, USA

Nicholas W, Arena

nicholas.w.arena@jpl.nasa.gov

Roles: data curation

Affiliation: Jet Propulsion Laboratory, California Institute of Technology, Pasadena, CA, USA

Renato P.M. Frasson

https://orcid.org/0000-0003-4299-1730

rfrasson@jpl.nasa.gov

Role: investigation

Affiliation: Jet Propulsion Laboratory, California Institute of Technology, Pasadena, CA, USA

Samantha C. Niemoeller

samantha.c.niemoeller@jpl.nasa.gov

Roles: software, visualization

Affiliation: Jet Propulsion Laboratory, California Institute of Technology, Pasadena, CA, USA

Simran S. Sangha

simran.s.sangha@jpl.nasa.gov

Roles: validation

Affiliation: Jet Propulsion Laboratory, California Institute of Technology, Pasadena, CA, USA

Steven Chan

https://orcid.org/0000-0001-6731-0079

steventsz.k.chan@jpl.nasa.gov

Roles: project administration, supervision, investigation

Affiliation: Jet Propulsion Laboratory, California Institute of Technology, Pasadena, CA, USA

References

Ahmad, S. K., Hossain, F., Eldardiry, H., & Pavelsky, T. M. (2020). A Fusion Approach for Water Area Classification Using Visible, near Infrared and Synthetic Aperture Radar for South Asian Conditions. IEEE Transactions on Geoscience and Remote Sensing, 58(4), 2471-2480. doi:10.1109/TGRS.2019.2950705

Beveridge, C., Hossain, F., & Bonnema, M. (2020). Estimating Impacts of Dam Development and Landscape Changes on Suspended Sediment Concentrations in the Mekong River Basin's 3S Tributaries. Journal of Hydrologic Engineering, 25(7). doi:10.1061/(ASCE)HE.1943-5584.0001949

Bjerklie, D. M., Birkett, C. M., Jones, J. W., Carabajal, C., Rover, J. A., Fulton, J. W., & Garambois, P. A. (2018). Satellite remote sensing estimation of river discharge: Application to the Yukon River Alaska. Journal of Hydrology, 561, 1000-1018. doi:10.1016/j.jhydrol.2018.04.005

Brown, J., Loveland, T. R., Ohlen, D., & Zhu, Z. (2003). LBA Regional Land Cover from AVHRR, 1-km, Version 1.2 (IGBP). In: ORNL Distributed Active Archive Center.

Buchhorn, M., Smets, B., Bertels, L., De Roo, B., Lesiv, M., Tsendbazar, N.-E., & Herold, M. F., S. . (2020). Copernicus Global Land Service: Land Cover 100m: collection 3: epoch 2019.

Büttner, G., Kosztra, B., Kleeschulte, S., Hazeu, G., Schröder, C., & AndreasLittkopf. (2018). Corine Global Land Cover 2018. Retrieved from: https://land.copernicus.eu/pan-european/corine-land-cover

CEC. (2020). North American land Cover. Retrieved from: http://www.cec.org/north-american-environmental-atlas/land-cover-30m-2020/

Chen, S., Huang, W., Chen, Y., & Feng, M. (2021). An adaptive thresholding approach toward rapid flood coverage extraction from sentinel-1 SAR imagery. Remote Sensing, 13(23). doi:10.3390/rs13234899

Dewitz, J. (2019). National Land Cover Database (NLCD) 2016 Products (ver. 2.0, July 2020).

Du, Y. Y., & Zhou, C. H. (1998). Automatically extracting remote sensing information for water bodies. Journal of Remote Sensing, 19(2), 5.

Duffie, J. A., & Beckman, W. A. (2013). Solar Engineering of Thermal Processes: Wiley.

ESA. (2016). CCI Land Cover - S2 land cover prototype of africa 2016. Retrieved from: https://climate.esa.int/en/projects/land-cover/about/

Feyisa, G. L., Meilby, H., Fensholt, R., & Proud, S. R. (2014). Automated Water Extraction Index: A new technique for surface water mapping using Landsat imagery. Remote Sensing of Environment, 140, 23-35. doi:10.1016/j.rse.2013.08.029

Friedl, M., & Sulla-Menashe, D. (2019). MCD12Q1 MODIS/Terra+Aqua Land Cover Type Yearly L3 Global 500m SIN Grid V006.

Gaines, M. D., Tulbure, M. G., & Perin, V. (2022). Effects of Climate and Anthropogenic Drivers on Surface Water Area in the Southeastern United States. Water Resources Research, 58(3). doi:10.1029/2021WR031484

Huang, W., Devries, B., Huang, C., Jones, J., Lang, M., & Creed, I. (2017). Automated extraction of inland surface water extent from Sentinel-1 data. Paper presented at the International Geoscience and Remote Sensing Symposium (IGARSS).

Ji, L., Zhang, L., & Wylie, B. (2009). Analysis of dynamic thresholds for the normalized difference water index. Photogrammetric Engineering and Remote Sensing, 75(11), 1307-1317. Retrieved from http://www.scopus.com/inward/record.url?eid=2-s2.0-72449164909&partnerID=40&md5=1417d50e1607212ddf5e68337d498b96

Jones, J. W. (2011). Remote sensing of vegetation pattern and condition to monitor changes in Everglades biogeochemistry. . Critical Reviews in Environment and Technology Special Edition, 41((S1)), 27.

Jones, J. W. (2015). Efficient Wetland Surface Water Detection and Monitoring via Landsat: Comparison with in situ Data from the Everglades Depth Estimation Network. Remote Sensing, 7(9). doi:10.3390/rs70912503

Jones, J. W. (2019). Improved automated detection of subpixel-scale inundation-revised Dynamic Surface Water Extent (DSWE) partial surface water tests. Remote Sensing, 11(4). doi:10.3390/rs11040374

Kreith, F., & Kreider, J. F. (1978). Principles of solar engineering. United States: Hemisphere Publishing Corporation,Washington, DC.

Masek, J. G., Ju, J., Claverie, M., Skakun, S., Roger, J.-C., Vermote, E., . . . Dungan, J. L. (2021). Hamronlized Landsat Sentineal-2 (HLS) Product User Guide Prouct Version 2.0. Greenbelt, MD: NASA

Otsu, N. (1979). Athreshold selecction method from gray-level histograms. IEEE Transactions on Systems, Man, and Cybernetics, 9, 5. doi:https://doi.org/10.1109/TSMC.1979.4310076

Owusu, C., Snigdha, N. J., Martin, M., & Kalyanapu, A. (2022). PyGEE-SWToolbox: A Python Jupyter Notebook Toolbox for Interactive SurfaceWater Mapping and Analysis Using Google Earth Engine. Sustainability, 14. doi:10.3390/su14052557

Perin, V., Tulbure, M. G., Gaines, M. D., Reba, M. L., & Yaeger, M. A. (2021). On-farm reservoir monitoring using Landsat inundation datasets. Agricultural Water Management, 246. doi:10.1016/j.agwat.2020.106694

Perin, V., Tulbure, M. G., Gaines, M. D., Reba, M. L., & Yaeger, M. A. (2022). A multi-sensor satellite imagery approach to monitor on-farm reservoirs. Remote Sensing of Environment, 270. doi:10.1016/j.rse.2021.112796

Petrakis, R. E., Soulard, C.E., Waller, E.K., Walker, J.J. (2022). Analysis of surface water trends for the conterminous United States using MODIS satellite data, 2003–2019. Water Resources Research, 58. doi:https://doi.org/10.1029/2021WR031399

Pickens, A. H., Hansen, M. C., Hancher, M., Stehman, S. V., Tyukavina, A., Potapov, P., . . . Sherani, Z. (2020). Mapping and sampling to characterize global inland water dynamics

from 1999 to 2018 with full Landsat time-series. Remote Sensing of Environment, 243. doi:10.1016/j.rse.2020.111792

Rowe, J. C., Duarte, A., Pearl, C. A., McCreary, B., Haggerty, P. K., Jones, J. W., & Adams, M. J. (2021). Demography of the Oregon spotted frog along a hydrologically modified river. Ecosphere, 12(6). doi:10.1002/ecs2.3634

Shiroma, G., Lavalle, M., & Buckley, S. (2022). An Area-Based Projection Algorithm for SAR Radiometric Terrain Correction and Geocoding. IEEE Transactions on Geoscience and Remote Sensing, 60, 1-1. doi:10.1109/TGRS.2022.3147472

Soulard, C. E., Walker, J. J., & Petrakis, R. E. (2020). Implementation of a surfacewater extent model in cambodia using cloud-based remote sensing. Remote Sensing, 12(6). doi:10.3390/rs12060984

Taylor, J. B., Sullivan, J. D., Teitelbaum, C. S., Reese, J. G., & Prosser, D. J. (2022). Comparing Landsat Dynamic Surface Water Extent to alternative methods of measuring inundation in developing waterbird habitats. Remote Sensing Applications: Society and Environment, 28, 100845. doi:https://doi.org/10.1016/j.rsase.2022.100845

Tucker, C. J. (1979). Red and Photographic infrared linear combinations for monitoring vegetation. Remote Sensing of Environment, 8, 127-150.

USGS. (2019). Landsat Dynamic Surface Water Extent. (LSDS-1325). Sioux Falls, SD: EROS Retrieved from https://d9-wret.s3.us-west-2.amazonaws.com/assets/palladium/production/s3fs-public/atoms/files/LSDS-1325-LandsatDynamicSurfaceWaterExtent_AlgorithmDescriptionDocument-v1.pdf

USGS. (2022). Land Change Monitoring, Assessment, and Proejction (LCMAP) Collection 1.3 Science Product Guide. Sioux Falls, SD: USGS

Vanderhoof, M. K., Christensen, J., Beal, Y. J. G., DeVries, B., Lang, M. W., Hwang, N., . . . Jones, J. W. (2020). Isolating anthropogenic wetland loss by concurrently tracking inundation and land cover disturbance across the Mid-Atlantic Region, U.S. Remote Sensing, 12(9). doi:10.3390/RS12091464

Viger, R. J., Hay, L. E., Jones, J. W., & Buell, G. R. (2010). Effects of including surface depressions in the application of the Precipitation-Runoff Modeling System in the Upper Flint River Basin, Georgia. Retrieved from Denver:

Walker, J. J., Soulard, C. E., & Petrakis, R. E. (2020). Integrating stream gage data and Landsat imagery to complete time-series of surface water extents in Central Valley, California. International Journal of Applied Earth Observation and Geoinformation, 84. doi:10.1016/j.jag.2019.101973

Xu, H. (2006). Modification of normalised difference water index (NDWI) to enhance open water features in remotely sensed imagery. International Journal of Remote Sensing, 27(14), 3025-3033. Retrieved from http://www.scopus.com/inward/record.url?eid=2-s2.0-33747136902&partnerID=40&md5=0a2ba3da05c4b50ddaa17d6b23896c50

Yang, Q., Shen, X., Anagnostou, E. N., Mo, C., Eggleston, J. R., & Kettner, A. J. (2021). A high-resolution flood inundation archive (2016–the present) from sentinel-1 SAR imagery over CONUS. Bulletin of the American Meteorological Society, 102(5), E1064-E1079. doi:10.1175/BAMS-D-19-0319.1